Article

Cell Reports

CD89 Is a Potent Innate Receptor for Bacteria and Mediates Host Protection from Sepsis

Graphical Abstract

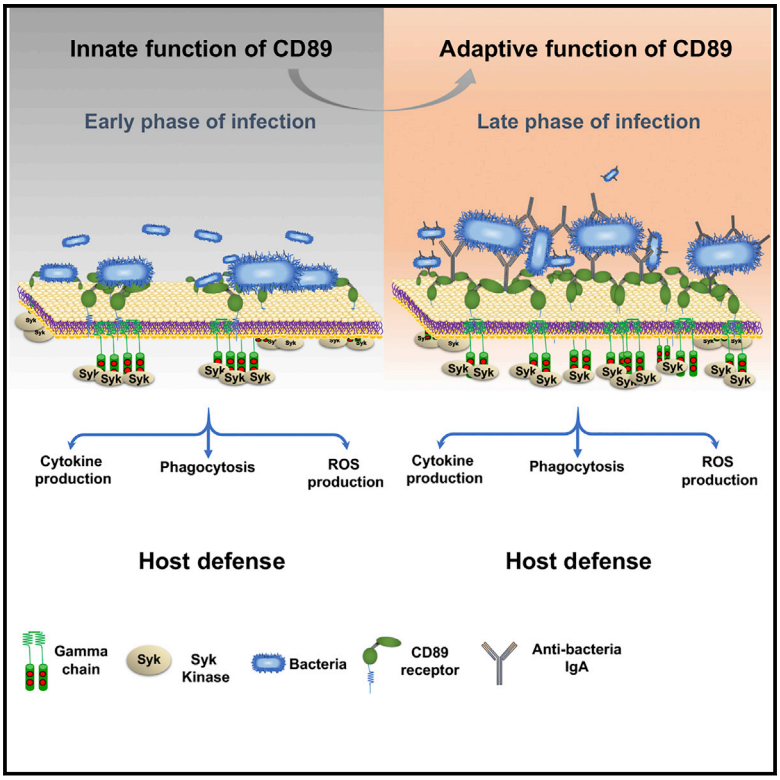

Highlights

- CD89 directly binds *Streptococcus pneumoniae* and *Escherichia coli*
- CD89 acts as an innate receptor before adaptive responses take place
- CD89 protects from sepsis by inducing innate immune responses against infections

Authors

Christian de Tymowski, Nicholas Heming, Mario D.T. Correia, ..., Marc Benhamou, Renato C. Monteiro, Sanae Ben Mkaddem

Correspondence

sanae.benmkaddem@inserm.fr

In Brief

de Tymowski et al. demonstrate that CD89 serves as an innate receptor during the early phase of infection. During the late phase, the receptor acts in both innate and adaptive immune responses through double interaction with IgA- or CRP-opsonized and non-opsonized bacteria.

de Tymowski et al., 2019, Cell Reports *27*, 762–775
April 16, 2019
https://doi.org/10.1016/j.celrep.2019.03.062

CellPress

OPEN ACCESS
CellPress

Cell Reports
Article

CD89 Is a Potent Innate Receptor for Bacteria and Mediates Host Protection from Sepsis

Christian de Tymowski,[1,2,3,4,11] Nicholas Heming,[1,2,3,4,11] Mario D.T. Correia,[5] Lilia Abbad,[1,2,3,4] Nathalie Chavarot,[1,2,3,4] Marie-Bénédicte Le Stang,[1,2,3,4] Heloise Flament,[1,2,3,4] Julie Bex,[1,2,3,4] Erwan Boedec,[1,2,3,4] Carine Bounaix,[1,2,3,4] Rafael Soler-Torronteras,[1,2,3,4] Erick Denamur,[3,6] Lionel Galicier,[7,8] Eric Oksenhendler,[7,8] Hans Joerg Fehling,[9] Fabiano Pinheiro da Silva,[5] Marc Benhamou,[1,2,3,4] Renato C. Monteiro,[1,2,3,4,10] and Sanae Ben Mkaddem[1,2,3,4,12,*]

[1]INSERM U1149, Centre de Recherche sur l'Inflammation, Paris, France
[2]CNRS ERL8252, Paris, France
[3]Université Paris Diderot, Sorbonne Paris Cité, Faculté de Médecine, Site Xavier Bichat, Paris, France
[4]Inflamex Laboratory of Excellence, Paris, France
[5]Emergency Medicine Department, Medical School, University of São Paulo, São Paulo, Brazil
[6]INSERM U1137, IAME, Paris, France
[7]Department of Clinical Immunology, Hôpital Saint-Louis, Assistance Publique Hôpitaux de Paris (APHP), Paris, France
[8]EA3518, Université Paris Diderot Paris 7, Paris, France
[9]Institute of Immunology, University Clinics Ulm, Heidelberg, Germany
[10]Service d'Immunologie, DHU Fire, Assistance Publique de Paris, Hôpital Bichat-Claude Bernard, Paris, France
[11]These authors contributed equally
[12]Lead Contact
*Correspondence: sanae.benmkaddem@inserm.fr
https://doi.org/10.1016/j.celrep.2019.03.062

SUMMARY

Direct bacterial recognition by innate receptors is crucial for bacterial clearance. Here, we show that the IgA receptor CD89 is a major innate receptor that directly binds bacteria independently of its cognate ligands IgA and c-reactive protein (CRP). This binding is only partially inhibited by serum IgA and induces bacterial phagocytosis by CD11c$^+$ dendritic cells and monocytes and/or macrophages, suggesting a physiological role in innate host defense. Blood phagocytes from common variable immunodeficiency patients bind, internalize, and kill bacteria in a CD89-dependent manner, confirming the IgA independence of this mechanism. *In vivo*, CD89 transgenic mice are protected in two different models of sepsis: a model of pneumonia and the cecal ligation and puncture (CLP) polymicrobial model of infection. These data identify CD89 as a first-line innate receptor for bacterial clearance before adaptive responses can be mounted. Fc receptors may emerge as a class of innate receptors for various bacteria with pleiotropic roles.

INTRODUCTION

Innate immunity is activated after recognition of pathogen-associated molecular patterns or structures that are not normally found in the host (Medzhitov, 2007). Phagocytes are equipped with several cell surface receptors that recognize pathogens directly. These innate immune receptors, such as Toll-like receptors (TLRs) (Takeda and Akira, 2001), the macrophage mannose receptor, the class A scavenger macrophage receptor MARCO (Mukouhara et al., 2011), or lectin-like molecules, trigger a variety of responses depending on the receptor and the cell type (van Egmond et al., 2000): (1) internalization of the pathogen, (2) activation of microbial killing mechanisms such as production of reactive oxygen species (ROS), (3) production of inflammatory cytokines and chemokines that orchestrate the development of adaptive immunity. Dysfunction of the innate immune response may lead to sepsis (Lozano et al., 2012). Sepsis is a complex syndrome defined as systemic inflammation in response to infection and resulting in organ failure (Singer et al., 2016). Bacteria are a frequent cause of sepsis and include both Gram-negative and Gram-positive pathogens (Deutschman and Tracey, 2014).

Antibody-mediated protection depends on complement and Fc receptors (FcRs), expressed predominantly by myeloid cells, initiating distinct signaling pathways (Pinheiro da Silva et al., 2008; Reth, 1989). These transmembrane receptors often contain one or more cytoplasmic immunoreceptor tyrosine-based activation motifs (ITAMs). Multimeric ligation of these receptors leads to tyrosine phosphorylation of ITAMs by Src family kinases (Abram and Lowell, 2007), in turn leading to recruitment of the tyrosine kinase Syk followed by cell activation (Bezbradica and Medzhitov, 2012; Humphrey et al., 2005). Several activating functions, such as phagocytosis, cytokine release, superoxide release, and bacterial killing, depend on ITAM integrity (Abram and Lowell, 2007). ITAM-bearing FcRs thus emerge as key cellular determinants for antibody-mediated defenses against bacterial infections. By contrast, an ITAM-bearing FcR, CD16A, can bind *Escherichia coli* (*E. coli*) directly without a requirement for opsonins, inducing an inhibitory signal through incomplete tyrosine phosphorylation of its ITAM and recruitment of the tyrosine phosphatase SHP-1 (Pinheiro da Silva et al., 2007). This ITAM-inhibitory (ITAMi) signaling pathway (Mkaddem et al., 2017; Blank et al., 2009; Getahun and Cambier, 2015; Hamerman and Lanier, 2006; Pasquier et al., 2005) results

in blockade of *E. coli* phagocytosis and sepsis (Pinheiro da Silva et al., 2007). Whether this CD16A-*E. coli* interaction is unique or could be extended to other FcRs and bacteria and whether they could play other than deleterious roles are major questions that remain unanswered.

Here we report that CD89, another ITAM-bearing FcR (Monteiro and Van De Winkel, 2003) that, like CD16A, mediates dual activating or inhibitory ITAM signaling (Pasquier et al., 2005; Rossato et al., 2015), captures Gram-negative *E. coli* on human phagocytes in the absence of its cognate ligands. Contrary to CD16A, CD89-*E. coli* interaction induces cell activation and plays a protective role in humanized CD89 transgenic mice through increased clearance and killing of these pathogens. In addition, both CD16A and CD89 bind non-opsonized Gram-positive *S. pneumoniae* (*S.p*), and both protect mice against lung infection.

RESULTS

CD89 Interacts Directly with Gram-Positive or Gram-Negative Bacteria

Because CD16A interacts directly with *E. coli* (Beppler et al., 2016; Pinheiro da Silva et al., 2007), we investigated whether another FcR distinct from FcγRs, CD89 (Pasquier et al., 2005; Rossato et al., 2015), might similarly interact with various bacteria in the absence of opsonins. Increasing soluble recombinant CD89 (sCD89) concentrations bound dose-dependently to *S.p* and *E. coli* (Figures 1A and 1B). However, only weak CD89 binding was observed with *Streptococcus pyogenes* or *S. aureus* (Figure 1C). Recently, two peptides from *E. coli* surface proteins that interact with CD16A have been identified; one of them is WzxE (Beppler et al., 2016). To investigate whether CD89 and bacteria interact through WzxE, we used WzxE$^{-/-}$ *E. coli* mutants. There was no difference in the interaction between wild-type (WT) or WzxE$^{-/-}$ *E. coli* and CD89, demonstrating that *E. coli* interacts with CD89 independently of WzxE (Figure 1C). Moreover, the CD89-bacteria binding was not due to an active uptake of CD89-detecting antibodies by bacteria because it was observed regardless of whether the bacteria were dead or alive (Figure 1D).

To examine whether transmembrane CD89 can bind bacteria, we took advantage of the *in vitro* binding capacity of labeled *S.p* or *E. coli* to bone marrow-derived macrophages (BMMs) isolated from CD89 transgenic animals (Launay et al., 2000) in the absence of the exogenous CD89 ligands immunoglobulin A (IgA) and CRP. *S.p* bound 4-fold more to BMMs derived from CD89 transgenic (CD89^{Tg}) animals than to BMMs obtained from littermates (Figure 1E). Similarly, *E. coli* bound 2-fold more to CD89^{Tg} BMMs (Figure 1F). Binding of both *S.p* and *E. coli* to CD89^{+} BMMs, but not to BMMs from littermates, was markedly inhibited by MIP8a, an anti-human CD89 blocking monoclonal antibody (mAb) (Figures 1G and 1H), demonstrating involvement of the IgA-binding site on CD89 for these interactions. For *S.p*, full inhibition of receptor interaction required higher a concentration of MIP8a or sCD89 (500–1,000 μg/mL) (Figures S1A and S1B). Moreover, sCD89 blocked *S.p* or *E. coli* interactions not only with CD89^{+} cells but also, to some extent, with CD89^{-} cells, suggesting that sCD89 binding to bacteria may disturb bacteria binding to other innate receptors (Figures 1G and 1H). Similar to BMMs, CD89 expression on CD11c^{+} bone marrow dendritic cells (BMDCs) increased bacterial phagocytosis, which was significantly inhibited by MIP8a (Figure S1C).

Bacterium-CD89 Interaction on Mouse Macrophages Induces Cell Activation, Bacterial Phagocytosis, and Bacterial Killing, which Are Dependent on the FcRγ Chain

Interaction of CD89^{Tg} BMMs with *S.p* in the absence of cognate CD89 ligands resulted in a strong increase in the mRNA expression and protein production of interleukin-6 (IL-6) and tumor necrosis factor alpha (TNF-α) but not of IL-1. *E. coli* induced mRNA expression and protein production of IL-6 and TNF-α, whereas, for IL-1, despite no difference in mRNA expression, an increase in IL-1β protein production was observed in CD89^{Tg} BMMs (Figures 2A, 2B, S1D, and S1E). Caspase-1-dependent posttranscriptional modifications of IL-1β may explain these differences, as reported by others (Bakema et al., 2015). To determine whether ITAM-dependent signaling is required for these responses, we used BMMs from a transgenic mouse expressing a genetically modified version of CD89, CD89$_{R209L}$, bearing a Leu instead of an Arg at position 209 in the transmembrane region (R209L). This mutant receptor cannot associate with the ITAM-bearing FcRγ signaling subunit (Launay et al., 1999). CD89$_{R209L}{}^{Tg}$ BMMs bound to both bacterial species similarly as CD89^{Tg} cells, indicating that the CD89-FcRγ interaction is not essential for bacterial binding (Figure S2). However, CD89-mediated cytokine production was completely dependent on the associated ITAM-bearing FcRγ subunit because CD89$_{R209L}{}^{Tg}$ BMMs failed to upregulate IL-6 and TNF-α secretion (Figures 2A and 2B). To evaluate the role of innate receptors and FcRs on differential bacterial capture, we assessed, by flow cytometry, the membrane expression on BMMs of TLRs 1, 2, 3, 4, 5, 6, and 8, the mannose receptor, MARCO, CD16, CD32, and CD64 (Figures S3A–S3C). Membrane expression of TLRs, FcRs, the mannose receptor, and MARCO showed no significant difference between WT and CD89^{Tg} BMMs before or after stimulation, showing that they are not responsible for the difference in bacterial capture observed between these cells.

To examine the phagocytic role of CD89 following interaction with bacteria, we performed an *E. coli* phagocytosis assay using the pH-sensitive fluorescent dye (pHrodo) labeling system. Cells from CD89^{Tg} mice internalized significantly more *E. coli* than cells from littermates, and this was inhibited by MIP8a F(ab')$_2$ and sCD89 in a dose-dependent manner (Figure 2C). This indicates that direct *E. coli* binding to CD89 results in bacterial phagocytosis and delivery to phago-lysosomes in the absence of IgA opsonins. Next we assessed whether this led to increased ROS production and bacterial killing. Live *S.p* or *E. coli* induced robust upregulation of ROS production by CD89^{Tg} BMMs that was dependent on the FcRγ chain because it was fully absent in CD89$_{R209L}{}^{Tg}$ cells, where it reached levels comparable with the ones observed in cells from littermates (Figure 2D). Killing of *S.p* or *E. coli* by CD89^{Tg} BMMs was significantly higher compared with that by BMMs derived from littermate or CD89$_{R209L}{}^{Tg}$ animals (Figure 2E). The number of live bacteria

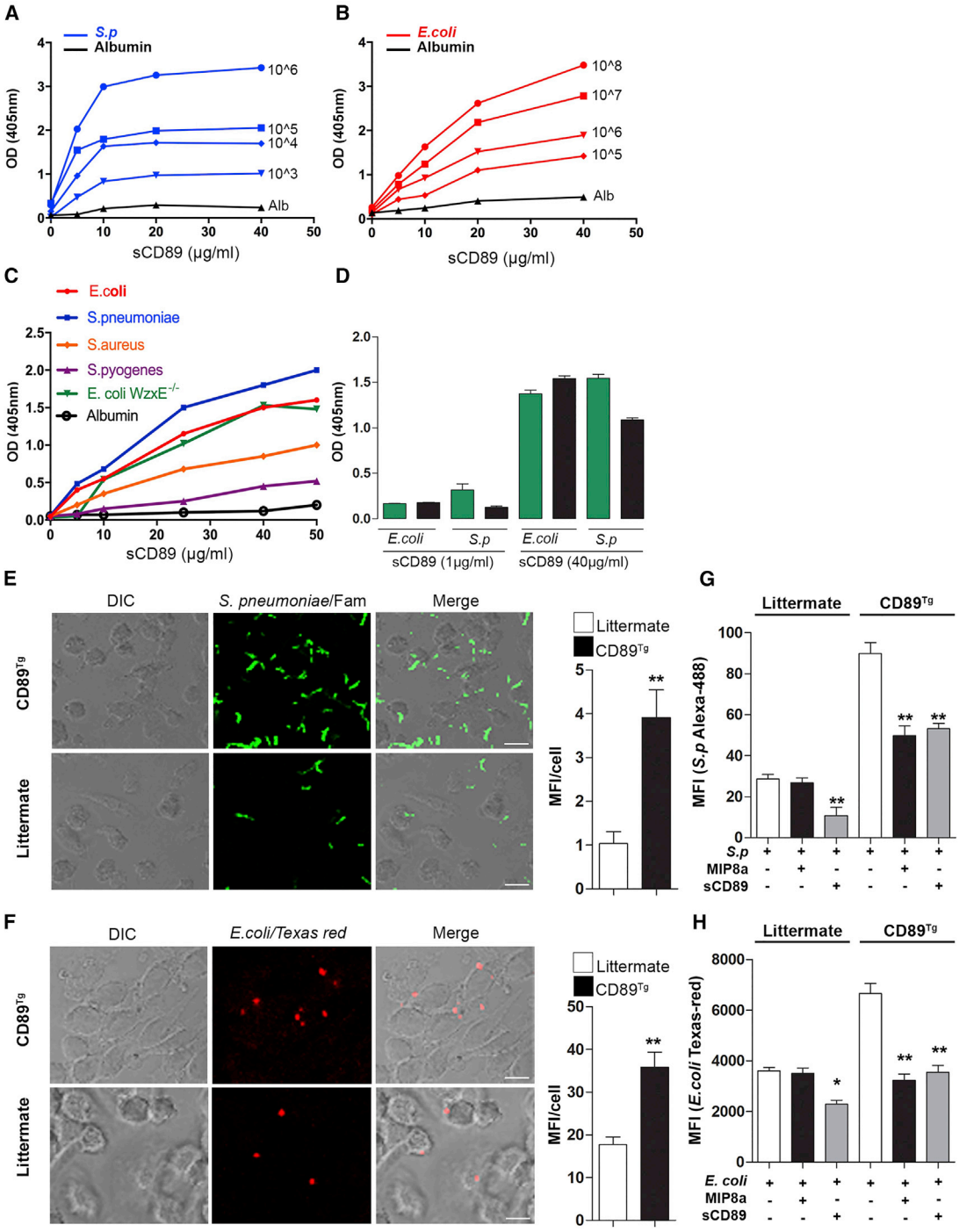

Figure 1. The Recombinant Soluble CD89 Receptor Interacts Directly with Bacteria

(A and B) Dose-dependent binding of soluble recombinant CD89 (sCD89) to fixed *S.p* (A) and *E. coli* (B). Binding to albumin (Alb) was used as a control.

(C) Comparison of sCD89 binding to various types of fixed bacteria.

(D) Interaction of sCD89 with live (green bar) versus fixed (black bars) 10^6 *E. coli* or 10^6 *S. p*.

(E and F) *S.p* (E) and *E. coli* (F) binding to BMMs grown from CD89 transgenic mice ($CD89^{Tg}$) or from littermates, visualized by confocal laser-scanning microscopy. Right: quantification of binding (n = 4). All data are presented as mean ± SEM. **p < 0.01, t test.

(G and H) *S.p* (G) and *E. coli* (H) binding to BMMs isolated from $CD89^{Tg}$ mice or from littermates in the presence or absence of the anti-CD89 blocking antibody MIP8a $F(ab')_2$ (10 µg/mL) or of sCD89 (500 µg/mL), analyzed by flow cytometry. MFI, mean fluorescence intensity. Data are presented as mean ± SEM; n = 5. *p < 0.05, **p < 0.01; t test.

See also Figure S1.

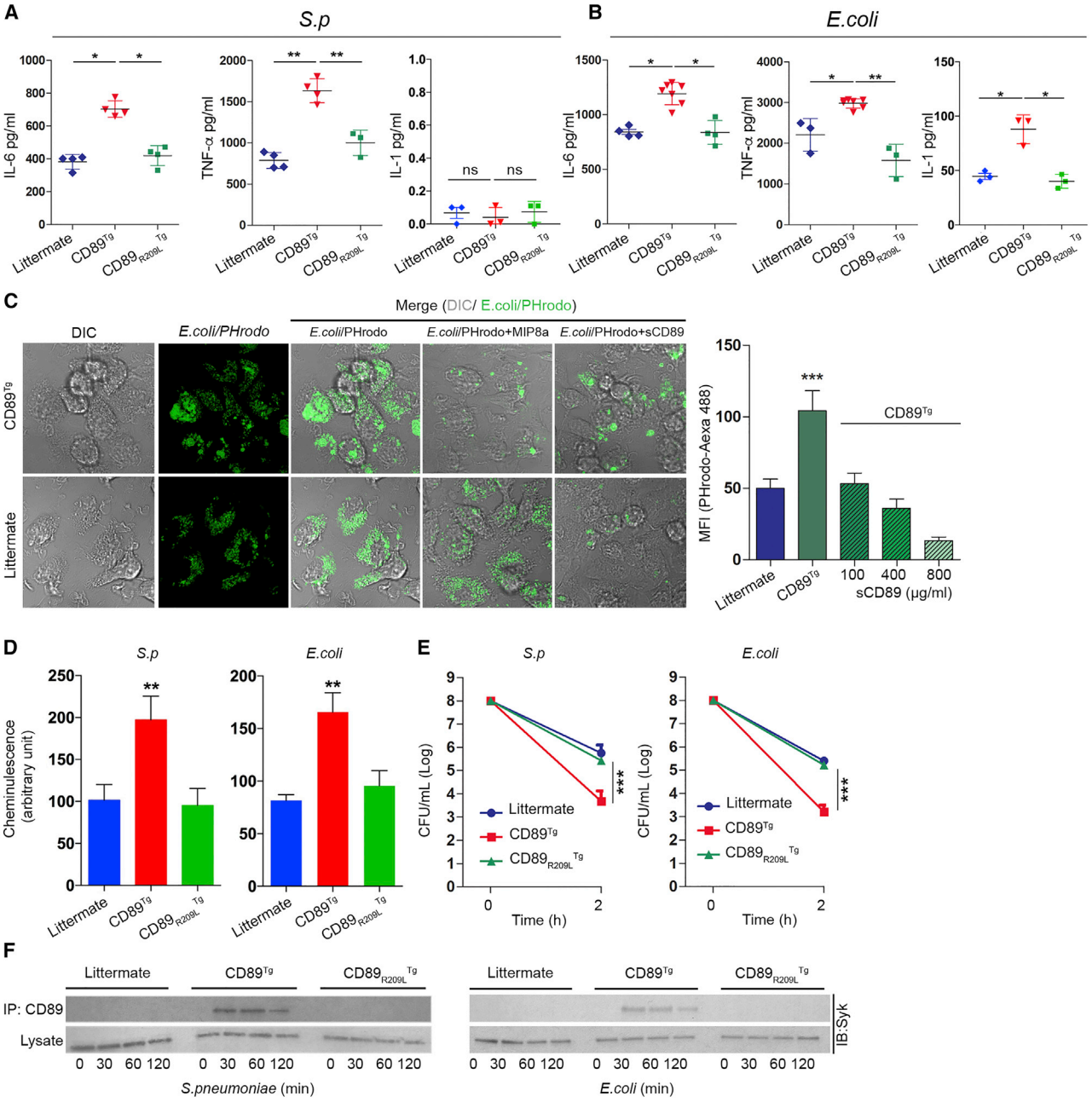

Figure 2. Bacterium-CD89 Interaction on Mouse Cells Induces Activating ITAM Signaling, Leading to Inflammatory Cytokine Production, Bacterial Phagocytosis, and Killing

(A and B) IL-6, TNF-α, and IL-1 production in the supernatant of BMMs obtained from $CD89^{Tg}$ and $CD89_{R209L}$ transgenic mice and littermate controls. Cells were incubated for 16 h in the presence of *S.p* (A) and *E. coli* (B) and cytokines in the supernatants were measured by ELISA. All data are presented as mean ± SEM; n = 3. *p < 0.05, **p < 0.01; t test.

(C) Confocal analysis of *E. coli*-pHrodo phagocytosis by BMMs obtained from $CD89^{Tg}$ mice compared with littermates in the presence or absence of MIP8a $F(ab')_2$ or sCD89 in a dose-dependent manner (100–800 μg/mL). Left: representative images. Right: quantification. Data are presented as mean ± SEM; n = 3. ***p < 0.001, t test.

(D) ROS production over 30 min by littermate, $CD89^{Tg}$, and $CD89_{R209L}$ transgenic BMMs stimulated by live *S.p* (left) or *E. coli* (right), measured by confocal microscopy. All data are presented as mean ± SEM; n = 15. **p < 0.01, t test.

(E) Quantification of bacterial survival after 2 h of incubation with BMMs from $CD89^{Tg}$, $CD89_{R209L}{}^{Tg}$, and littermate mice. Data are presented as mean ± SEM; n = 3. ***p < 0.001, t test.

(legend continued on next page)

decreased by 100-fold in $CD89^{Tg}$ BMM cultures compared with littermate and $CD89_{R209L}{}^{Tg}$ cells within 2 h of infection. To explore the signaling pathway involved, we analyzed the recruitment of Syk to CD89 following stimulation of BMMs obtained from $CD89^{Tg}$ or littermate mice by either *S.p* or *E. coli.* Bacterium-CD89 interaction resulted in sustained recruitment of Syk (lasting a minimum of 2 h) to the FcRγ-associated CD89, whereas $CD89_{R209L}{}^{Tg}$ BMMs failed to induce such recruitment (Figure 2F). Syk recruitment to CD89 but not of SHP-1 (Figure S4A) following bacterium stimulation was also observed in cultured human blood monocytes and was inhibited by addition of sCD89 (Figure S4B). Together, these results indicate that bacterium-CD89 interaction results in induction of the FcRγ ITAM signaling pathway, leading to stable Syk recruitment and cell activation with bacterial phagocytosis and killing.

IgA-Deficient CVID Phagocytes Mediate Phagocytosis, ROS Production, and Bacterial Killing through CD89 Interaction

To further demonstrate that CD89-bacterium interaction occurs independently of IgA, we examined human blood phagocytes from healthy donors (HDs) and from severe common variable immunodeficiency disorder (CVID) patients who were totally deficient in plasma IgA (Table S1). CD89 expression on blood monocytes and neutrophils was maintained (Figure 3A) and even significantly increased (Figures S5A and S5B) in CVID patients compared with HDs. *S.p* and *E. coli* binding to cells from CVID patients or HDs was dependent on CD89 because they were inhibited by MIP8a $F(ab')_2$ and by non-specific human IgA (ns-IgA; devoid of anti-bacterium antibody activity) (Figures 3B and S5C). As expected, specific human IgA (plasma-derived IgA [pd-IgA]) significantly increased phagocytosis (Figure S5D). Therefore, although pd-IgA can serve as an opsonin, binding of *S.p* and *E. coli* to CD89 does not require IgA.

To confirm the phagocytic and activating role of native human CD89 toward bacteria independent of IgA, we performed an *E. coli* pHrodo phagocytosis assay followed by anti-bacterial responses in blood monocytes purified from CVID patients. Culture-derived macrophages from CVID patient monocytes efficiently phagocytosed labeled *E. coli* similar to HD cells (Figure 3C). Moreover, MIP8a $F(ab')_2$ markedly decreased bacterial phagocytosis, confirming that CD89-bacterium interaction was functional even in the absence of human IgA. This was associated with efficient cytokine and ROS production (Figures 3D and 3E), which were inhibited by MIP8a $F(ab')_2$. Finally, culture-derived macrophages from CVID patients performed bacterial killing in a similar manner as cells from healthy individuals (Figure 3F). Of note, MIP8a $F(ab')_2$ blocked more than 80% of cell activation, suggesting that, although it blocks the interaction between bacteria and CD89, it induces, at the same time, inhibition of cell activation by scavenger and innate immune receptors, in agreement with others (Watanabe et al., 2011).

Taken together, these findings indicate that CD89-bacterium interaction results in essential FcR-activating functions (phagocytosis, cytokine and ROS production, and bacterial killing) that are preserved in human blood phagocytes from IgA-deficient CVID patients, suggesting that CD89 may play a direct protective role against *E. coli* and *S.p* infection in the absence of IgA.

Role of CD89-Bacterium Interaction under Physiological Conditions

To address the physiological role of CD89-bacterium interaction, we examined whether it was prevented by competition with physiological concentrations of ns-IgA. Both *S.p* and *E. coli* binding were inhibited by ns-IgA (which does not present any anti-bacterial activity) in a dose-dependent manner (Figure 4A), demonstrating that bacterial binding on CD89 was hindered by IgA binding to the CD89 D1 domain. However, this inhibition was partial and reached a plateau of 80% inhibition above 700 μg/mL IgA, allowing a significant remaining portion of sCD89 to bind bacteria despite physiological concentrations of IgA (up to 2 mg/mL). As expected, bacterium-CD89 binding was increased in the presence of IgA displaying anti-bacterium antibody activity acting as opsonins (Figure 4B). To further determine whether the remaining binding of bacteria to CD89 observed in the presence of physiological concentrations of IgA could be functionally relevant, we explored bacterium capture in the presence of 2 mg/mL ns-IgA or of the MIP8a $F(ab')_2$ fragment. The strong increase in bacterium capture observed in $CD89^{Tg}$ BMMs was significantly reduced in the presence of physiological concentrations of ns-IgA or in the presence of MIP8a $F(ab')_2$. However, it remained increased by 50% to 100% compared with bacterium capture by BMMs derived from littermate animals (Figure 4C), confirming CD89 as a potent innate receptor for bacteria. Monocytes and/or macrophages are not the only immune cells expressing CD89. Among these other $CD89^{+}$ cells, a subset of immature dendritic cells, notably epidermal Langerhans cells, can capture bacteria in sites that have low IgA antibody concentrations (Geissmann et al., 2001; Pasquier et al., 2004). Similar to BMMs, CD89 expression on $CD11c^{+}$ BMDCs significantly enhanced bacterial phagocytosis compared with BMDCs from littermates (Figures 4D and 4E). This enhancement remained strong (around a 100% increase) even under physiological concentrations of ns-IgA or with MIP8a $F(ab')_2$ (Figures 4D, S1C, and 5C). Altogether, these experiments suggest that CD89-bacterium direct interaction can be effective in the interior milieu and, hence, may play a physiological role in the host.

CD89-Bacterium Interaction Protects against Mortality in Two Sepsis Models

To investigate the *in vivo* role of the direct interaction between bacteria and CD89 on bacterial clearance, we used experimental pneumonia caused by intranasal infection with *S.p*, a Gram-positive coccus (Lu et al., 2008). $CD89^{Tg}$ mice exhibited significantly

(F) Induction of CD89-ITAM signaling by *S.p* or *E. coli.* After incubation of BMMs from littermate, $CD89^{Tg}$, or $CD89_{R209L}{}^{Tg}$ mice with 10^6 colony-forming units (CFUs) of *S.p* (top) or *E. coli* (bottom) for the indicated times, co-immunoprecipitated proteins by A77 anti-CD89 mAb (top) and total proteins (bottom) were analyzed by immunoblot (IB) using rabbit polyclonal anti-Syk antibody.
See also Figures S1–S4.

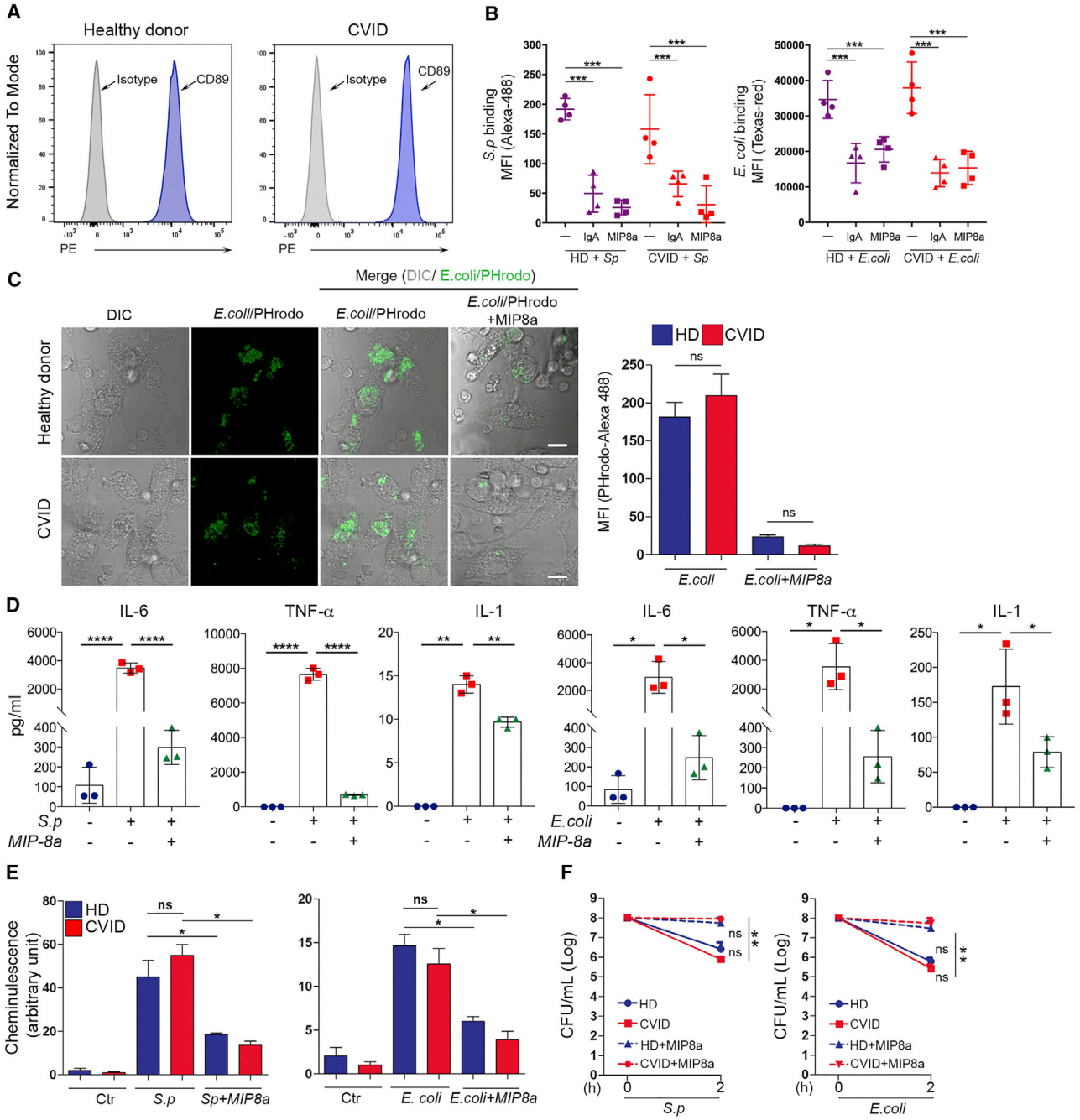

Figure 3. IgA-Deficient CVID Phagocytes Mediate Phagocytosis, ROS Production, and Bacterial Killing through CD89 Interaction

(A) Representative plots of CD89 expression on blood monocytes isolated from healthy donors (HDs) (left) and CVID patients (right) using a phycoerythrin (PE)-conjugated anti-CD89 antibody and its isotype control.

(B) Binding of *S.p* or *E. coli* to blood monocytes from HDs (purple symbols) or from CVID patients (red symbols) in the presence of monomeric IgA (500 μg/mL) or of MIP8a F(ab')$_2$ (10 μg/mL). All data are presented as mean ± SEM; n = 4. ***p < 0.001, t test.

(C) Phagocytosis of *E. coli*-pHrodo by human blood monocytes and/or macrophages isolated from HDs or from CVID patients. Left: representative images. Scale bars, 200 μm. Right: quantification (n = 3). All data are presented as mean ± SEM. ns, not significant.

(D) IL-6, TNF-α, and IL-1 production in the supernatant of monocytes obtained from CVID patients. Cells were incubated for 16 h in the presence of *E. coli* or *S.p* and in the presence or absence of MIP8a F(ab')$_2$ (500 μg/mL), and cytokines in the supernatants were measured by ELISA. All data are presented as mean ± SEM; n = 3. *p < 0.05, **p < 0.01, ****p < 0.0001; t test.

(legend continued on next page)

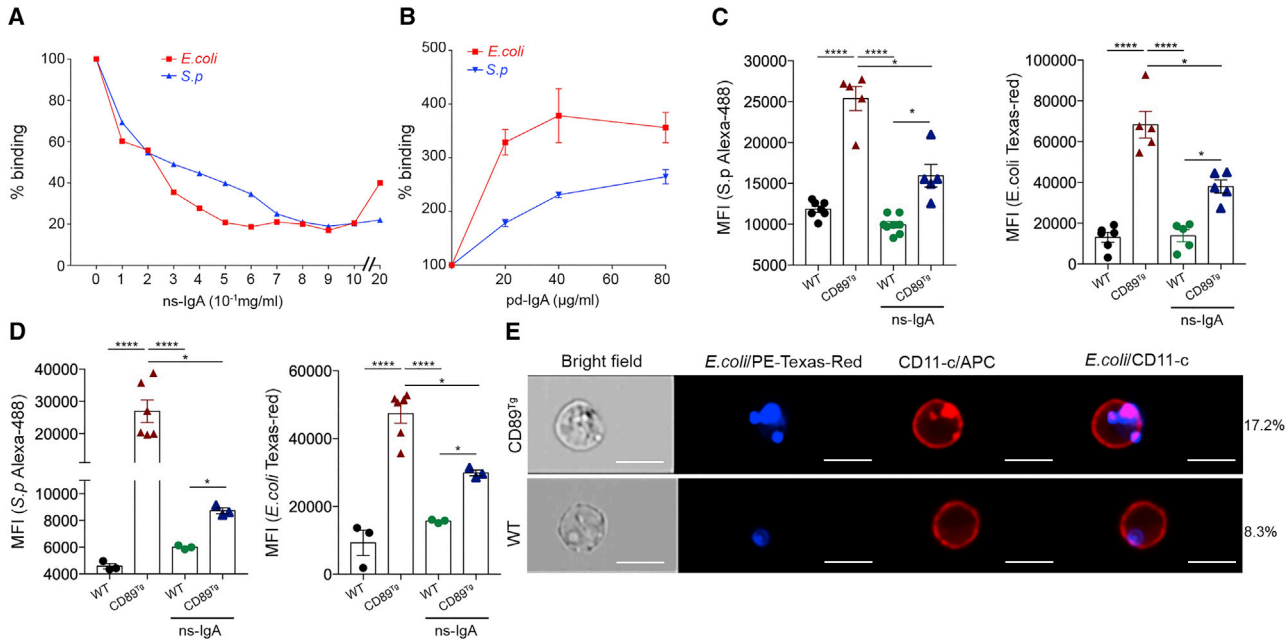

Figure 4. Role of CD89-Bacterium Interaction under Physiological Conditions

(A) Competitive ELISA assays between sCD89 and *S.p* (blue line) or *E. coli* (red line) and ns-IgA.

(B) Competitive ELISA assays between sCD89 and *S.p* (blue line) or *E. coli* (red line) and pd-IgA.

(C) Bacterial phagocytosis by BMMs obtained from CD89^{Tg} mice (left) compared with littermates (right). Bacteria were allowed to be phagocytosed by BMMs from the indicated mice in the presence or absence of ns-IgA at physiological concentration (2 mg/mL) or MIP8a F(ab)'$_2$ (500 μg/mL). Cells were washed and analyzed by flow cytometry. Data are presented as mean ± SEM; n = 3. *p < 0.05, ***p < 0.001; t test.

(D) *S.p* (left) or *E. coli* (right) phagocytosis by BMDCs obtained from CD89^{Tg} mice compared with littermates. Bacteria were allowed to be phagocytosed by BMDCs from the indicated mice in the presence or absence of ns-IgA at physiological concentration (2 mg/mL). Cells were washed and analyzed by flow cytometry. Data are presented as mean ± SEM; n = 3. *p < 0.05, ***p < 0.0001; t test.

(E) Representative images of *E. coli* (blue) and CD11c (red) staining by BMDCs derived from CD89^{Tg} or wild-type (WT) mice captured by imaging flow cytometry (scale bars, 5 μm) and the percentages of the bacterial phagocytosis score.

See also Figures S1C and S5C.

lower mortality following infection relative to littermates (Figure 5A). The number of live *S.p* in the lungs of CD89^{Tg} animals was 100-fold lower 48 h post-inoculation compared with littermates (Figure 5B), in agreement with the increased bactericidal and phagocytic CD89-dependent activity in phagocytes from the former animals, as described above. CD89^{Tg} mice showed less interstitial and peribronchiolar infiltration as well as less alveolitis (Figures 5C and 5D). Alveolar spaces were infiltrated by monomorphic cells, but these cells were seen in markedly higher numbers in non-transgenic littermates. Moreover, CD89^{Tg} mice expressed higher local mRNA levels of the inflammatory cytokine IL-1 6 h after bacterial inoculation, but this early inflammation resolved more rapidly, with the level of IL-1 mRNA showing a trend to lower levels in CD89^{Tg} animals 48 h post-infection compared with littermates (Figure 5E). In contrast, IL-6 levels significantly increased in littermates compared with transgenic mice 6 h and 48 h after infection. This suggests that the level of IL-6 is associated with the severity of sepsis. However, the level of TNF-α mRNA was identical in the two groups at 6 h and 48 h.

To extend the protective role of CD89 to polymicrobial infections, we assessed the consequences of CD89 expression in a severe model of peritonitis induced by CLP. As in the pneumonia model, CD89^{Tg} mice were significantly protected from sepsis (Figure 5F). The peritoneum of CD89^{Tg} mice contained a lower number of total bacteria, *E. coli*, and *Enterococcus* (the major strains identified by MALDI-TOF) than littermates after CLP (Figures 5G–5I). CD89^{Tg} mice expressed early and transient IL-1 and TNF-α responses in the peritoneum post-CLP compared with the delayed responses observed in WT animals (Figure 5J). These early responses were associated with markedly lower mortality rates. Taken together, these results indicate that, following CLP, CD89 triggered by gut-residing bacteria induces more efficient phagocytosis with a better controlled and rapid pro-inflammatory response, resulting in decreased bacterial numbers in the peritoneum and more effective protection of

(E) Production of ROS in response to co-incubation of HD or CVID human monocytes with *S.p or E. coli* in the presence or absence of MIP8a F(ab)'$_2$. Experiments were performed as in (D). All data are presented as mean ± SEM; n = 3. *p < 0.05, t test.

(F) Bacterial survival after incubation with HD or CVID human monocytes for 2 h in the presence or absence of MIP8a F(ab)'$_2$ as in (E) (n = 3). Data are presented as mean ± SEM; n = 4. **p < 0.01.

See also Figure S5 and Table S1.

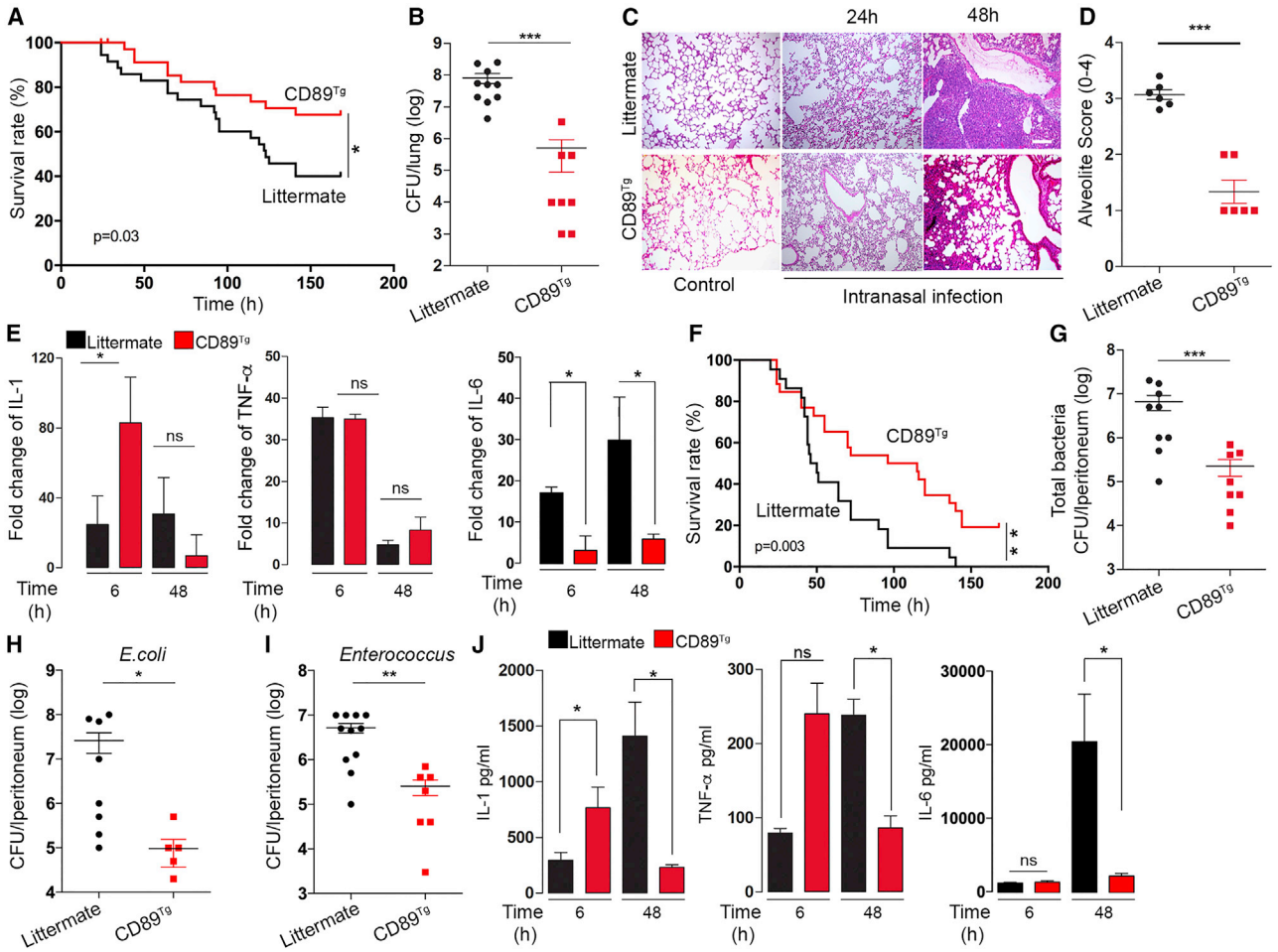

Figure 5. CD89-Bacterium Interaction Protects against Infection-Related Mortality in Mice

(A) Survival of CD89^{Tg} mice (red line) and littermates (black line) after intranasal inoculation (at time 0) with *S. pneumonia* (n = 25). Kaplan-Meier curves and log rank test were used to compare mortality rates. All data are presented as mean ± SEM. *p < 0.05.

(B) Decreased lung contents of *S.p* in CD89 transgenic compared with littermate mice. All data are presented as mean ± SEM; n = 8. ***p < 0.001, t test.

(C) H&E staining of lung sections from representative CD89^{Tg} and littermate animals after intranasal infection. Scale bars, 200 μm.

(D) Alveolitis invasion score of monomorphic inflammatory cells. All data are presented as mean ± SEM; n = 6. ***p < 0.001, t test.

(E) mRNA expression of cytokines (IL-1, TNF-α, and IL-6) was assessed by qRT-PCR of 5 independent lung tissue RNA samples collected 6 and 48 h after intranasal infection. mRNA levels were normalized to β-actin mRNA levels. All data are presented as mean ± SEM; n = 6. *p < 0.05, t test.

(F) Increased survival of CD89^{Tg} mice (red line, n = 26) compared with littermates (black line, n = 22) after CLP. Kaplan-Meier curves and log rank test were used to compare mortality rates. All data are presented as mean ± SEM. **p < 0.01.

(G–I) 48 h after CLP, peritoneal fluid was evaluated for total bacteria (G), *E. coli* (H), and *Enterococcus* (I) in CD89^{Tg} mice and littermates. All data are presented as mean ± SEM. *p < 0.05, **p < 0.01, ***p < 0.001; t test.

(J) IL-1, TNF-α, and IL-6 levels in peritoneal lavage, assessed by ELISA 6 and 48 h after CLP. All data are presented as mean ± SEM; n = 3. *p < 0.05, t test.

See also Figures S6A–S6C.

the host. As in the *S.p* model, IL-6 increased only in littermates compared with CD89^{Tg} mice 48 h post-CLP, confirming the deleterious role of IL-6 in sepsis, and the level of this cytokine may be a biomarker of sepsis severity.

To confirm that CD89 can protect against sepsis induced by Gram-negative bacteria, we used the sepsis model of intraperitoneal *E. coli* injection. As in the pneumonia and CLP models, CD89^{Tg} mice were protected to a great extent from sepsis (Figure S6A). The peritonea of CD89^{Tg} animals contained a lower number of bacteria than those of littermates after 48 h of infection (Figure S6B). CD89^{Tg} mice expressed early and transient IL-1 and TNF-α responses in the peritoneum post-infection compared with the delayed responses observed in WT animals (Figure S6C).

CD89 Protection against Sepsis Is Dependent on the FcRγ Chain

Because the CD89-associated FcRγ chain was mandatory for the CD89-dependent bactericidal activity of phagocytes (cf. data described above), we performed similar infection experiments using CD89$_{R209L}$^{Tg} mice to determine whether FcRγ was also required for the protection observed *in vivo*. No difference in mortality with littermates was observed in intranasal infection with *S.p*

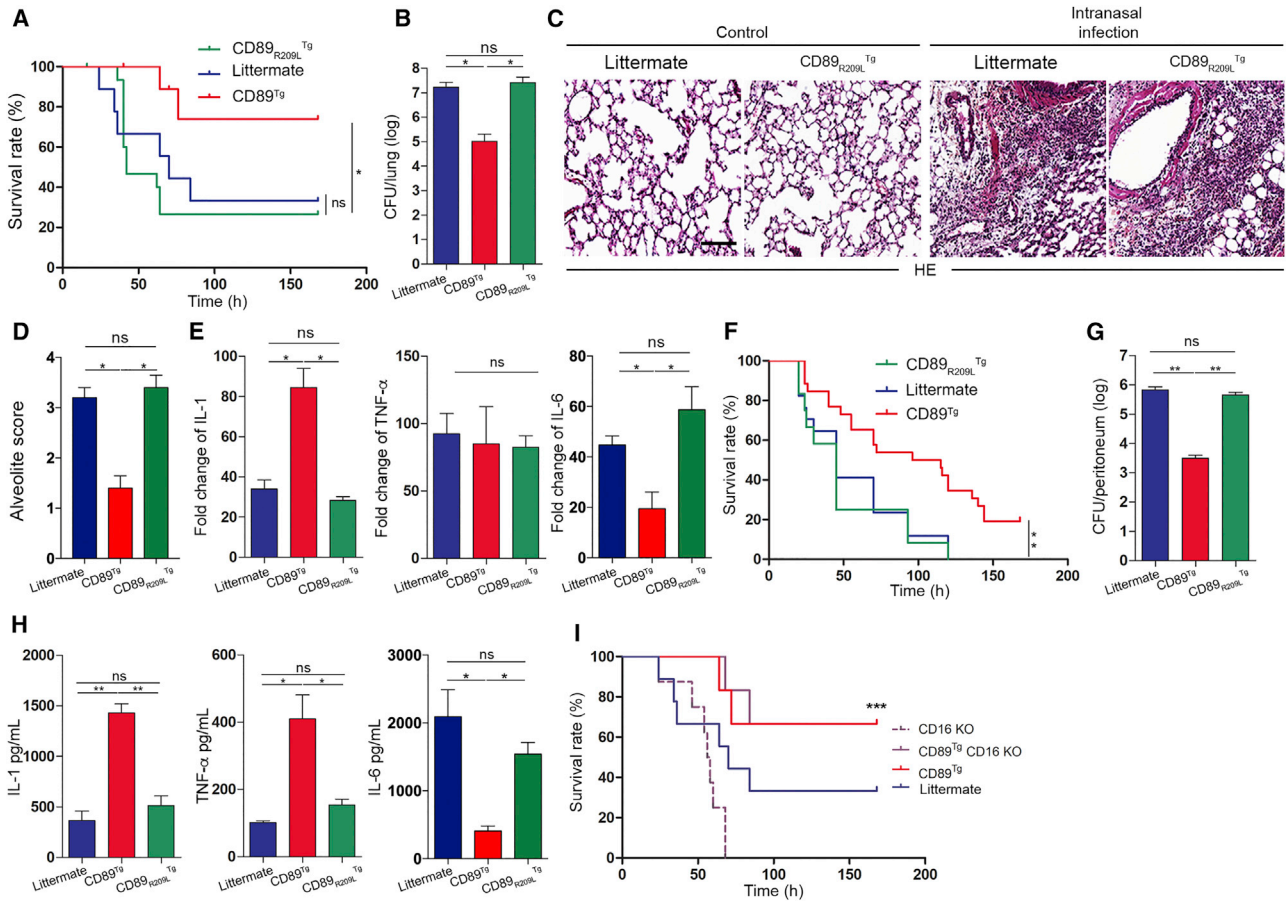

Figure 6. CD89 Protects against Sepsis through the FcRy Chain-Dependent Pathway

(A) Increased survival of $CD89^{Tg}$ animals after lung infection by intranasal inoculation with *S.p* compared with $CD89_{R209L}{}^{Tg}$ animals or littermates. Kaplan-Meier curves and log rank test were used to compare mortality rates. All data are presented as mean ± SEM; n = 10. *p < 0.05, t test.

(B) Decreased lung counts of *S.p* in $CD89^{Tg}$ compared with $CD89_{R209L}{}^{Tg}$ animals or littermates (n = 5). All data are presented as mean ± SEM. *p < 0.05, t test.

(C) H&E staining of lung sections from representative $CD89_{R209L}{}^{Tg}$ mice and littermates after intranasal infection. Scale bars, 200 μm.

(D) Alveolitis invasion score of monomorphic inflammatory cells. All data are presented as mean ± SEM. *p < 0.05, t test.

(E) mRNA expression of IL-1, TNF-α, and IL-6 in RNA samples collected 6 h after intranasal inoculation from lung tissue of distinct mice. Cytokine mRNA levels were normalized to β-actin mRNA levels, as indicated in Figure 5E. Data are presented as mean ± SEM; n = 4. *p < 0.05, t test.

(F) Increased survival of $CD89^{Tg}$ mice (n = 10) compared with $CD89_{R209L}{}^{Tg}$ mice or littermates (n = 10) after CLP. Kaplan-Meier curves and log rank test were used to compare mortality rates. Data are presented as mean ± SEM. **p < 0.01.

(G) After 48 h of CLP, peritoneal fluid counts of bacteria were less numerous in the peritoneal fluid of $CD89^{Tg}$ mice than in that from $CD89_{R209L}{}^{Tg}$ or littermate animals (n = 5). All data are presented as mean ± SEM. **p < 0.01, t test.

(H) IL-1, TNF-α, and IL-6 levels in peritoneal lavage, assessed by ELISA 6 h after CLP. Data are presented as mean ± SEM; n = 5. *p < 0.05, **p < 0.01, t test.

(I) Survival rates of CD16 KO, CD16 KO-$CD89^{Tg}$, $CD89^{Tg}$, and littermate mice after intranasal *S.p* infection. Kaplan-Meier curves and log rank test were used to compare mortality rates. Data are presented as mean ± SEM. ***p < 0.001.

See also Figures S6D and S6E.

or after CLP (Figures 6A and 6F), indicating that bacterium interaction with $CD89_{R209L}$ is not protective. This was confirmed by similar bacterium numbers colonizing the infected tissues, similar alveolite scores, similar cytokine responses, and tissue injury in littermate and $CD89_{R209L}{}^{Tg}$ mice (Figures 6B–6E and 6F–6H).

CD89 Protects against Sepsis in the Absence of CD16 during Gram-Positive Infections

Because mouse CD16 interacts directly with *E. coli* (Figure S6D) and aggravates sepsis in the CLP model through induction of the ITAMi signal (Pinheiro da Silva et al., 2007), we examined whether it could also interact with *S.p*. CD16 readily interacted with these bacteria (Figure S6D) and protected mice against *S.p* pneumonia (Figure 6I), in contrast to its deleterious action in the CLP model (Figure S6E), demonstrating that CD16 plays opposite roles in sepsis depending on the type of bacteria and/or organs involved. We then explored whether CD89 could further protect mice beyond what has been observed in CD16-KO mice. In the pneumonia model, CD89 was protective regardless of the presence of CD16, demonstrating that its action did not rely on CD16 (Figure 6I). In CLP-induced sepsis, CD89 provided slightly supplemental protection (but did not

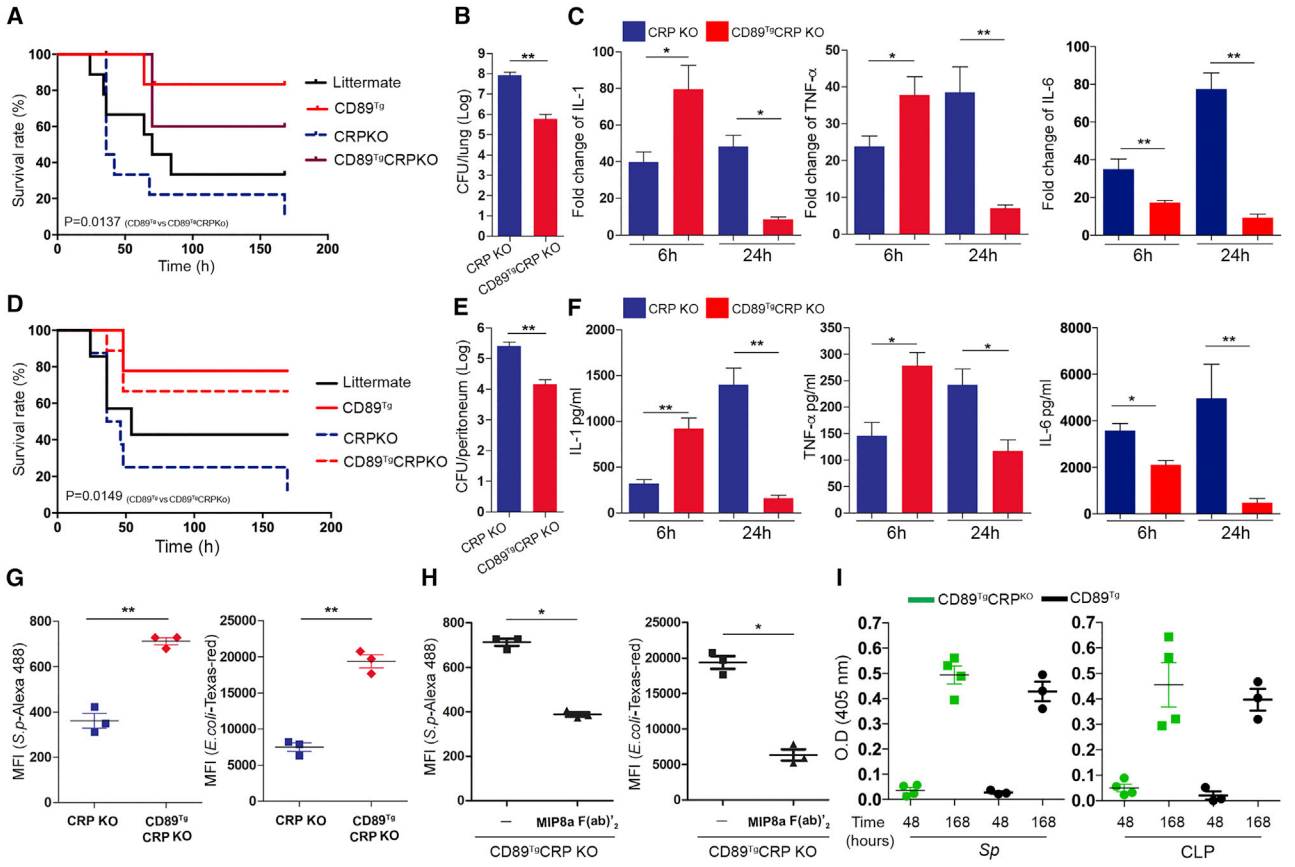

Figure 7. CD89 Protection against Sepsis Is Independent of CRP and IgA Antibodies during the Early Phase of Infection

(A) Increased survival of CD89^{Tg}CRP-KO animals after intranasal infection with *S.p* compared with CRP-KO mice (n = 12 per group). CD89^{Tg} mice and their littermates were used as controls. Kaplan-Meier curves and log rank test were used to compare mortality rates. All data are presented as mean ± SEM.

(B) Decreased lung counts of *S.p* in CD89^{Tg}CRP-KO mice at 48 h compared with CRP-KO mice (n = 4). All data are presented as mean ± SEM. **p < 0.01, t test.

(C) Expression of cytokine mRNA (IL-1, TNF-α, and IL-6) was assessed by qPCR of independent lung tissue RNA samples collected 6 and 24 h after intranasal infection. Cytokine mRNA levels were normalized to β-actin mRNA levels, as indicated in Figure 5E (n = 4). All data are presented as mean ± SEM. *p < 0.05, **p < 0.01; t test.

(D) Increased survival of CD89^{Tg}CRP-KO (n = 10) compared with CRP-KO mice (n = 10) after CLP. Kaplan-Meier curves and log rank test were used to compare mortality rates. CD89^{Tg} mice and their littermates were used as controls. All data are presented as mean ± SEM.

(E) Peritoneal fluid counts of bacteria 48 h after CLP (n = 4). All data are presented as mean ± SEM. **p < 0.01, t test.

(F) IL-1, TNF-α, and IL-6 levels in peritoneal lavage, assessed by ELISA 6 and 48 h after CLP (n = 4). All data are presented as mean ± SEM. *p < 0.05, **p < 0.01; t test.

(G) Phagocytosis of *S.p* (left) and *E. coli* (right) after incubation with BMMs isolated from CD89^{Tg}CRP-KO or CRP-KO mice.

(H) Phagocytosis of *S.p* (left) and *E. coli* (right) after incubation with BMMs isolated from CD89^{Tg}CRP-KO or CRP-KO mice in the presence of MIP8a anti-CD89 F(ab')$_2$. All data are presented as mean ± SEM. *p < 0.05, **p < 0.01; t test.

(I) Measurement of mouse IgA antibodies against the indicated bacteria 48 or 168 h after *S.p* infection (left) or CLP (right) in CD89^{Tg} or CD89^{Tg}CRP-KO mice. Data are presented as mean ± SEM.

See also Figure S7.

reach statistical significance) compared with that observed in the absence of CD16 (Figure S6E). Therefore, CD89 is a reliable receptor in immune defense against infection and may counterbalance the CD16-ITAMi inhibitory signal that is deleterious in the CLP model of acute peritonitis.

CD89-Mediated Protection against Sepsis Is Independent of CRP and Anti-bacterial IgA Antibodies

Because CRP is a known ligand for CD89 that could serve as an opsonin (Du Clos and Mold, 2011), we took advantage of CRP-knockout (KO) mice (Teupser et al., 2011) and backcrossed them to CD89^{Tg} mice. Similar to what we described above for WT and CD89^{Tg} mice, a significant increase in survival rates was obtained when the CD89 gene was introduced in the CRP-KO background (Figures 7A and 7D). This was associated with significant decreases in live bacterium counts in the lung and peritoneal cavities of CD89^{Tg}CRP-KO mice compared with CRP-KO mice (Figures 7B and 7E). This protection was associated with robust early inflammation (at 6 h), followed by efficient resolution of inflammation (at 48 h), as measured by the local

level of cytokine mRNA or proteins (IL-1, TNF-α, and IL-6) (Figures 7C and 7F). Phagocytosis assays showed a significant increase in bacterial phagocytosis in BMMs from CD89^{Tg}CRP-KO mice compared with CRP-KO mice that was inhibited by addition of MIP8a F(ab')$_2$ (Figures 7G and 7H), confirming the CRP-independent protective role of CD89. To exclude a role of mouse IgA antibodies in this protection through a putative interaction with human CD89 (mouse IgA interacts weakly with human CD89; Berthelot et al., 2012), we measured IgA anti-bacterial antibody levels at 48 h and on day 7 after infection. 48h after infection, when a significant increase in survival in CD89^{Tg}CRP-KO mice was already detectable ($p < 0.02$; Figures 7A and 7D), no anti-bacterial IgA was detected in the sera of both models of infected mice (intranasal infection and CLP) (Figure 7I).

Because the pentraxin CRP binds and activates CD89 (Lu et al., 2011), we also investigated the effect of an absence of CRP on bacteria binding to CD89. Because BMMs can produce CRP (Li et al., 2012), we used BMMs derived from WT or CRP$^{-/-}$ mice on the CD89^{Tg} background. The bacterial binding assay showed that both *S.p* and *E. coli* interact with CD89 independent of CRP and that these interactions were inhibited by MIP8a anti-CD89 F(ab')$_2$ (Figure S7A). In the CLP model, the level of CRP from CD89^{Tg} and WT mice increased slightly in the peritoneal exudate and doubled in serum 6 h after infection, reaching between 20 and 25 μg/mL without any difference between the two strains (Figures S7B and S7C). To formally exclude a role of CRP in CD89-mediated host protection, we explored whether 25 μg/mL CRP increased *E. coli* phagocytosis by CD89^{+} monocytes. This concentration had no effect on *E. coli* phagocytosis, whereas (as expected) a high level of CRP (200 μg/mL) increased it (Figure S7D). These results demonstrate that neither a different modulation of CRP expression by CD89 nor CRP itself are required for CD89-dependent protection against infection.

Additional analyses were performed to determine whether mouse IgA could be involved in CD89-mediated protection. At steady state, monocytes isolated from WT or CD89^{Tg} mice bound mouse IgA similarly (Figure S7E). BMMs isolated from CD89^{Tg} mice bound non-specific mouse IgA poorly but, as a positive control, readily bound ns-IgA. The low binding of mouse IgA was not increased by the presence of bacteria (Figure S7F). To explore the effects of mouse IgA-CD89 interaction, serum IgA binding to BMMs was compared between serum collected on day 1 and on day 7 from mice subjected to infection. IgA binding increased similarly on day 7 compared with day 1 in BMMs from WT and CD89Tg mice (Figure S7G). Therefore, no difference in mouse IgA binding could be detected between WT and CD89^{Tg} monocytes, and no bacterium-specific mouse IgA was detected early after infection, confirming that the CD89-dependent protection observed in our experimental settings did not involve mouse IgA. Taken together, these results identify CD89 as an innate immune receptor that could play a crucial role in host protection during the early phase of bacterial infection.

DISCUSSION

Our results demonstrate that CD89 binds both Gram-positive and Gram-negative bacilli in a direct opsonin-independent manner, resulting in increased protection against infection. In addition to IgA, CD89 also binds CRP, an acute-phase protein (Lu et al., 2011). Binding of CRP to CD89 on a binding site distinct from that of IgA induces activation of both macrophages and neutrophils, which play a major role in the innate response to infection. However, neither IgA nor CRP account for the CD89 interaction with bacteria described here because our *in vitro* and *ex vivo* studies were performed in the absence of both proteins and were confirmed *in vivo* in the absence of detectable IgA opsonins and of CRP.

Many innate immune receptors are involved in bacterium recognition by macrophages, including TLRs, MARCO, various lectins, and the IgG receptor CD16A. The fact that the sole additional presence of CD89 is capable *in vitro* to, at least, double the capture of bacteria (Figure 1), double the production of cytokines and of ROS, and decrease by 100-fold the number of bacteria surviving phagocytosis (Figure 2) reveals CD89 as a major player in antibacterial defense. These effects were confirmed in *in vivo* models where the number of bacteria collected in tissue 48 h after infection was reduced by 100-fold in CD89^{Tg} compared with WT mice together with a powerful increase in cytokine production and survival (Figure 5). However, this protection (survival) was lower than expected from the 90%–99% reduction of bacterial load observed in CD89^{Tg} mice. This suggests that, in our infection protocols, the bacterial loads were in large excess of what is necessary to induce sepsis and that, in infections with lower bacterial loads, the protection provided by CD89 could be more drastic. Although mouse IgA binds poorly to CD89 and should not compete with bacteria for CD89 binding, in humans, serum IgA inhibits bacteria binding to CD89 (Figure 3). However, human serum IgA does not completely block bacteria binding to CD89, as observed in the ELISA experiments depicted in Figure 3. Hence, a significant number of free CD89 would remain available for bacterial capture, allowing a physiological role of this interaction, notably by Langerhans cells, which are usually located in sites with a low IgA concentration. The fact that no bacterium-specific mouse IgA antibodies were detected in CD89^{Tg} and in CD89^{Tg}CRP-KO mice early (48 h) after infection (i.e., at a time when CD89-dependent protection was already strongly effective in these mice) indicates that CD89 is not only a receptor for bacteria but also that it may play an important role in innate immune responses against infection before adaptive responses take place (Figure 7I).

In our sepsis models, CD89 proved to be efficient in reducing the bacterial burden and in improving the survival of the animals. One can propose that the improved capture and killing of the bacteria, together with the increased early inflammatory reaction we observed, may favor robust and rapid mobilization of the innate immune system that can more efficiently contain bacterial invasion before it can get out of hand. This acceleration of the inflammatory reaction would also contribute to CD89-dependent resolution of inflammation.

The direct involvement of CD89 in innate immune responses adds a layer to the various functions of this receptor. Immune responses are controlled by a balance of antagonistic signals. This balance prevents tissue damage by ensuring the return of activated cells to their resting state. The CD89-IgA pair plays a major role in host defense as well as a dual role in immunity by mediating either activating or inhibitory responses. This dual activity

of CD89 is mirrored by the dual activity of serum IgA, which may exert either anti- or pro-inflammatory activity (Ben Mkaddem et al., 2013; Rossato et al., 2015). Anti-inflammatory signals are generated by CD89 upon binding of monomeric IgA, whereas pro-inflammatory CD89-dependent responses are induced by IgA immune complexes. The latter initiate multiple biological processes, including phagocytosis and antibody-dependent, cell-mediated cytotoxicity, leading to targeted bacterial lysis (Bakema and van Egmond, 2011). CD89 cross-linking by its ligand can also promote cell activation, resulting in release of cytokines, inflammatory mediators, and superoxide anions. Furthermore, pro-inflammatory cytokines induce CD89 expression on Kupffer cells of $CD89^{Tg}$ mice, leading to increased clearance of mouse IgA-coated bacteria (van Egmond et al., 2000). It has been proposed that interactions between serum IgA and CD89 on Kupffer cells may provide a ''second line of defense'' in mucosal immunity by eliminating invasive bacteria entering through the portal circulation. However, mouse IgA has a very low affinity for human CD89 (Berthelot et al., 2012), which, in agreement with our observations, would argue in favor of direct binding of bacteria to CD89 on Kupffer cells. This mechanism of defense would promote bacterial capture and subsequent macrophage activation through CD89 before the generation of specific IgA is completed. This would reinforce a prompt innate immune response before highly proliferative microbes overwhelm the immune system.

Although frequent infections are a hallmark of immunodeficiency, there are few studies comparing the frequency of infection between selective IgA-deficient (IgAD) and CVID patients and, unfortunately no data, to our knowledge, comparing different bacterial strains. It has been reported, however, that IgAD patients present less severe pulmonary infection compared with IgAD associated with IgG subclass deficiency (Björkander et al., 1985). In a recent study, it has been reported that, although prolonged, very low levels of IgG and/or IgM are associated with a heightened risk of infection, selective IgAD appears to be better tolerated by most patients (Furst, 2009). Our data regarding blood phagocytes from CVID patients with no IgA but reconstituted for IgG and IgM revealed that CD89 is upregulated and functional because it is able to mediate bacterial internalization and killing. These findings are in agreement with previous observations supporting the residual ability of IgAD patients to fight infection.

Interestingly, and in line with our study, CD89 expression and activation are increased in human blood phagocytes following bacterial infection, together with increased expression and association of FcRγ with CD89 (Chiamolera et al., 2001). Moreover, lipopolysaccharides (LPS) upregulate CD89 expression on blood monocytes (Shen et al., 1994). The fact that bacteria or bacterial products can increase CD89 expression is in line with our present data showing that CD89-mediated protection in mice also occurs in the absence of specific IgA antibodies on day 2, which led us to postulate that CD89 acts as an innate immune receptor in the early phase of infection, when individuals are not yet armed with specific antibodies. On the other hand, in the late phase of infection, when the IgA antibody responses are established, direct binding of CD89 to bacteria may further increase CD89 crosslinking by providing additional anchoring sites for the capture of opsonized bacteria, enhancing ITAM signaling, phagocytosis, and bacterial clearance. The existence of two means of bacterial capture by CD89 (IgA-dependent and IgA-independent) that may cooperate during the late phase of infection, when an IgA response has taken place, emphasizes the importance of this receptor in immunity.

Taking advantage of the balance between activating and inhibitory immune responses, micro-organisms are able to subvert the human immune system, inducing inhibitory signals to survive (Van Avondt et al., 2015). We previously observed that *E. coli* subvert CD16A signaling to evade the host immune system by inducing a potent ITAMi signal involving SHP-1, leading to sepsis. In contrast, in *S.p* infection, CD16A was required for protection. Further structural studies of the binding of the various bacterial species to CD16A will be necessary to elucidate the basis for these opposite signals. Interestingly, and in contrast to CD16A, binding of both *E. coli* and *S.p* to CD89 led to recruitment of Syk, bacterial phagocytosis, and controlled inflammation, as evidenced by the resolution of IL-1 production at 48 h in the pneumonia and CLP models and in the enhanced survival of $CD89^{Tg}$ mice. Of note, although both CD89 and CD16A are functionally associated with the FcRγ adaptor, their genes are located in different chromosomes, and there is no homology between the extracellular domains of these receptors (Monteiro and Van De Winkel, 2003), suggesting that differences in their extracellular domains may indeed account for their different behavior in the presence of *E. coli*. Additional studies will be necessary to shed light on this puzzling contrast. However, although CD16-KO mice were protected against CLP-mediated sepsis, $CD89^{Tg}$ mice (which still express CD16) were as protected as CD16-KO mice, arguing in favor of a different bacterium-binding site on these receptors. Hence, it is expected that non-opsonized bacteria bind both CD16A and CD89 on phagocytes. Our results show that the activating signal generated by CD89 can overcome the inhibitory signal generated by CD16A in the CLP model.

Altogether, our results suggest that CD89 fulfills an innate protective role against non-opsonized bacteria immediately after infection in the absence of specific IgA and in the presence of low basal levels of CRP. This role would progress further, taking advantage of rising CRP levels that would provide CRP opsonins for CD89 binding and would finally evolve to an immune-adaptive role when the adaptive IgA immune response has kicked in. Thus, CD89 should be considered a receptor with a complex and dynamic plasticity encompassing that of the immune response to infection.

Although WzxE protein from *E. coli* interacts with CD16 (Beppler et al., 2016), it failed to interact with CD89 because receptor binding to $WzxE^{-/-}$ mutant *E. coli* remained unchanged. This result argues in favor of a different *E. coli* binding site. Thus, it remains unknown which molecular determinants of the bacterial cell surface of *E. coli, S. aureus*, and *S.p* interact with CD89.

Several other questions arise from our study. For instance, what are the respective molecular determinants that allow bacterial binding to CD16A and to CD89, and are they shared between bacterial species and between these FcRs? Can these FcRs bind other pathogens, such as viruses, parasites, or

yeasts? Whatever answers to these questions may be provided in the future, our study, by demonstrating that at least two different FcRs are able to bind two different (Gram-positive and Gram-negative) non-opsonized bacterial species with various outcomes (protection or aggravation), allows one to contemplate whether FcRs can now emerge as a class of innate receptors and to speculate that this may have been their prime function early in evolution.

Overall, our findings expand the spectrum of signals able to activate cells through FcRs and open avenues for the treatment of bacterial infections, such as therapeutic interventions aimed at stimulating CD89 expression to boost anti-pathogen responses. This study uncovers the importance of the ITAM-bearing CD89 in innate immunity and in sepsis.

STAR★METHODS

Detailed methods are provided in the online version of this paper and include the following:

- KEY RESOURCES TABLE
- CONTACT FOR REAGENT AND RESOURCE SHARING
- EXPERIMENTAL MODEL AND SUBJECT DETAILS
  - Subjects
  - Animals
- METHOD DETAILS
  - Pneumonia and cecal ligation and puncture models
  - Cells, reagents and antibodies
  - Flow cytometry
  - Imaging flow cytometry
  - Protein expression on BMM membrane
  - Bacteria and microbiological culture
  - Bacterial invasion count
  - Bacterial binding and phagocytosis assays
  - Bacterial killing
  - Confocal laser scanning microscopy
  - ROS production assay on PMN by chemiluminescence
  - Immunoprecipitation and immunoblotting
  - Production of soluble proteins and antibodies
  - ELISA
  - Real-time PCR
- QUANTIFICATION AND STATISTICAL ANALYSIS

SUPPLEMENTAL INFORMATION

Supplemental Information can be found online at https://doi.org/10.1016/j.celrep.2019.03.062.

ACKNOWLEDGMENTS

The authors thank the confocal microscopy image facility. This work was supported by grants from ANR JC (ANR-17-CE17-0002-01), DIM1HEALTH "action financée par la Région Ile-de-France," and LabEx Inflamex (ANR-11-IDEX-0005-02). R.C.M. was supported by the Equipe Program of the Fondation pour la recherche médicale (FRM). C.d.T. was supported by FRM (41482). The authors thank Dr. Cedric Vonarburg and CSL Behring for providing human monomeric pdIgA. We are indebted to the patients and healthy volunteers who participated in the study.

AUTHOR CONTRIBUTIONS

C.d.T., N.H., M.D.T.C., L.A., N.C., E.B., J.B., R.S.-T., and C.B. performed experiments and analyzed data. H.J.F. generated CRP-KO mice. L.G. and E.O. provided human samples and analyzed data. E.D., M.B., and R.C.M. contributed to analysis of the data and editing of the manuscript. S.B.M. designed the research, analyzed data, and wrote the manuscript.

DECLARATION OF INTERESTS

The authors declare no competing interests.

Received: May 29, 2018
Revised: January 11, 2019
Accepted: March 15, 2019
Published: April 16, 2019

REFERENCES

Abram, C.L., and Lowell, C.A. (2007). The expanding role for ITAM-based signaling pathways in immune cells. Sci. STKE *2007*, re2.

Aloulou, M., Ben Mkaddem, S., Biarnes-Pelicot, M., Boussetta, T., Souchet, H., Rossato, E., Benhamou, M., Crestani, B., Zhu, Z., Blank, U., et al. (2012). IgG1 and IVIg induce inhibitory ITAM signaling through FcγRIII controlling inflammatory responses. Blood *119*, 3084–3096.

Bakema, J.E., and van Egmond, M. (2011). The human immunoglobulin A Fc receptor FcαRI: a multifaceted regulator of mucosal immunity. Mucosal Immunol. *4*, 612–624.

Bakema, J.E., Tuk, C.W., van Vliet, S.J., Bruijns, S.C., Vos, J.B., Letsiou, S., Dijkstra, C.D., van Kooyk, Y., Brenkman, A.B., and van Egmond, M. (2015). Antibody-opsonized bacteria evoke an inflammatory dendritic cell phenotype and polyfunctional Th cells by cross-talk between TLRs and FcRs. J. Immunol. *194*, 1856–1866.

Ben Mkaddem, S., Rossato, E., Heming, N., and Monteiro, R.C. (2013). Anti-inflammatory role of the IgA Fc receptor (CD89): from autoimmunity to therapeutic perspectives. Autoimmun. Rev. *12*, 666–669.

Ben Mkaddem, S., Hayem, G., Jönsson, F., Rossato, E., Boedec, E., Boussetta, T., El Benna, J., Launay, P., Goujon, J.M., Benhamou, M., et al. (2014). Shifting FcγRIIA-ITAM from activation to inhibitory configuration ameliorates arthritis. J. Clin. Invest. *124*, 3945–3959.

Beppler, J., Mkaddem, S.B., Michaloski, J., Honorato, R.V., Velasco, I.T., de Oliveira, P.S., Giordano, R.J., Monteiro, R.C., and Pinheiro da Silva, F. (2016). Negative regulation of bacterial killing and inflammation by two novel CD16 ligands. Eur. J. Immunol. *46*, 1926–1935.

Berthelot, L., Papista, C., Maciel, T.T., Biarnes-Pelicot, M., Tissandie, E., Wang, P.H., Tamouza, H., Jamin, A., Bex-Coudrat, J., Gestin, A., et al. (2012). Transglutaminase is essential for IgA nephropathy development acting through IgA receptors. J. Exp. Med. *209*, 793–806.

Bezbradica, J.S., and Medzhitov, R. (2012). Role of ITAM signaling module in signal integration. Curr. Opin. Immunol. *24*, 58–66.

Björkander, J., Bake, B., Oxelius, V.A., and Hanson, L.A. (1985). Impaired lung function in patients with IgA deficiency and low levels of IgG2 or IgG3. N. Engl. J. Med. *313*, 720–724.

Blank, U., Launay, P., Benhamou, M., and Monteiro, R.C. (2009). Inhibitory ITAMs as novel regulators of immunity. Immunol. Rev. *232*, 59–71.

Chiamolera, M., Launay, P., Montenegro, V., Rivero, M.C., Velasco, I.T., and Monteiro, R.C. (2001). Enhanced expression of Fc alpha receptor I on blood phagocytes of patients with gram-negative bacteremia is associated with tyrosine phosphorylation of the FcR-gamma subunit. Shock *16*, 344–348.

Conley, M.E., Notarangelo, L.D., and Etzioni, A.; Representing PAGID (Pan-American Group for Immunodeficiency) and ESID (European Society for Immunodeficiencies) (1999). Diagnostic criteria for primary immunodeficiencies. Clin. Immunol. *93*, 190–197.

Deutschman, C.S., and Tracey, K.J. (2014). Sepsis: current dogma and new perspectives. Immunity *40*, 463–475.

Du Clos, T.W., and Mold, C. (2011). Pentraxins (CRP, SAP) in the process of complement activation and clearance of apoptotic bodies through Fcγ receptors. Curr. Opin. Organ Transplant. *16*, 15–20.

Furst, D.E. (2009). Serum immunoglobulins and risk of infection: how low can you go? Semin. Arthritis Rheum. *39*, 18–29.

Geissmann, F., Launay, P., Pasquier, B., Lepelletier, Y., Leborgne, M., Lehuen, A., Brousse, N., and Monteiro, R.C. (2001). A subset of human dendritic cells expresses IgA Fc receptor (CD89), which mediates internalization and activation upon cross-linking by IgA complexes. J. Immunol. *166*, 346–352.

Getahun, A., and Cambier, J.C. (2015). Of ITIMs, ITAMs, and ITAMis: revisiting immunoglobulin Fc receptor signaling. Immunol. Rev. *268*, 66–73.

Hamerman, J.A., and Lanier, L.L. (2006). Inhibition of immune responses by ITAM-bearing receptors. Sci. STKE *2006*, re1.

Humphrey, M.B., Lanier, L.L., and Nakamura, M.C. (2005). Role of ITAM-containing adapter proteins and their receptors in the immune system and bone. Immunol. Rev. *208*, 50–65.

Kanamaru, Y., Arcos-Fajardo, M., Moura, I.C., Tsuge, T., Cohen, H., Essig, M., Vrtovsnik, F., Loirat, C., Peuchmaur, M., Beaudoin, L., et al. (2007). Fc alpha receptor I activation induces leukocyte recruitment and promotes aggravation of glomerulonephritis through the FcR gamma adaptor. Eur. J. Immunol. *37*, 1116–1128.

Launay, P., Patry, C., Lehuen, A., Pasquier, B., Blank, U., and Monteiro, R.C. (1999). Alternative endocytic pathway for immunoglobulin A Fc receptors (CD89) depends on the lack of FcRgamma association and protects against degradation of bound ligand. J. Biol. Chem. *274*, 7216–7225.

Launay, P., Grossetête, B., Arcos-Fajardo, M., Gaudin, E., Torres, S.P., Beaudoin, L., Patey-Mariaud de Serre, N., Lehuen, A., and Monteiro, R.C. (2000). Fcalpha receptor (CD89) mediates the development of immunoglobulin A (IgA) nephropathy (Berger's disease). Evidence for pathogenic soluble receptor-Iga complexes in patients and CD89 transgenic mice. J. Exp. Med. *191*, 1999–2009.

Leijh, P.C., van den Barselaar, M.T., van Zwet, T.L., Daha, M.R., and van Furth, R. (1979). Requirement of extracellular complement and immunoglobulin for intracellular killing of micro-organisms by human monocytes. J. Clin. Invest. *63*, 772–784.

Li, M., Liu, J.T., Pang, X.M., Han, C.J., and Mao, J.J. (2012). Epigallocatechin-3-gallate inhibits angiotensin II and interleukin-6-induced C-reactive protein production in macrophages. Pharmacol. Rep. *64*, 912–918.

Lozano, R., Naghavi, M., Foreman, K., Lim, S., Shibuya, K., Aboyans, V., Abraham, J., Adair, T., Aggarwal, R., Ahn, S.Y., et al. (2012). Global and regional mortality from 235 causes of death for 20 age groups in 1990 and 2010: a systematic analysis for the Global Burden of Disease Study 2010. Lancet *380*, 2095–2128.

Lu, J., Marnell, L.L., Marjon, K.D., Mold, C., Du Clos, T.W., and Sun, P.D. (2008). Structural recognition and functional activation of FcgammaR by innate pentraxins. Nature *456*, 989–992.

Lu, J., Marjon, K.D., Marnell, L.L., Wang, R., Mold, C., Du Clos, T.W., and Sun, P. (2011). Recognition and functional activation of the human IgA receptor (FcalphaRI) by C-reactive protein. Proc. Natl. Acad. Sci. USA *108*, 4974–4979.

Lucas, M., Lee, M., Lortan, J., Lopez-Granados, E., Misbah, S., and Chapel, H. (2010). Infection outcomes in patients with common variable immunodeficiency disorders: relationship to immunoglobulin therapy over 22 years. J. Allergy Clin. Immunol. *125*, 1354–1360.e4.

Martinez, J.E., Romero-Steiner, S., Pilishvili, T., Barnard, S., Schinsky, J., Goldblatt, D., and Carlone, G.M. (1999). A flow cytometric opsonophagocytic assay for measurement of functional antibodies elicited after vaccination with the 23-valent pneumococcal polysaccharide vaccine. Clin. Diagn. Lab. Immunol. *6*, 581–586.

Medzhitov, R. (2007). Recognition of microorganisms and activation of the immune response. Nature *449*, 819–826.

Mkaddem, S.B., Murua, A., Flament, H., Titeca-Beauport, D., Bounaix, C., Danelli, L., Launay, P., Benhamou, M., Blank, U., Daugas, E., et al. (2017). Lyn and Fyn function as molecular switches that control immunoreceptors to direct homeostasis or inflammation. Nat. Commun. *8*, 246.

Monteiro, R.C., and Van De Winkel, J.G. (2003). IgA Fc receptors. Annu. Rev. Immunol. *21*, 177–204.

Monteiro, R.C., Cooper, M.D., and Kubagawa, H. (1992). Molecular heterogeneity of Fc alpha receptors detected by receptor-specific monoclonal antibodies. J. Immunol. *148*, 1764–1770.

Mukouhara, T., Arimoto, T., Cho, K., Yamamoto, M., and Igarashi, T. (2011). Surface lipoprotein PpiA of Streptococcus mutans suppresses scavenger receptor MARCO-dependent phagocytosis by macrophages. Infect. Immun. *79*, 4933–4940.

Pasquier, B., Lepelletier, Y., Baude, C., Hermine, O., and Monteiro, R.C. (2004). Differential expression and function of IgA receptors (CD89 and CD71) during maturation of dendritic cells. J. Leukoc. Biol. *76*, 1134–1141.

Pasquier, B., Launay, P., Kanamaru, Y., Moura, I.C., Pfirsch, S., Ruffié, C., Hénin, D., Benhamou, M., Pretolani, M., Blank, U., and Monteiro, R.C. (2005). Identification of FcalphaRI as an inhibitory receptor that controls inflammation: dual role of FcRgamma ITAM. Immunity *22*, 31–42.

Pinheiro da Silva, F., Aloulou, M., Skurnik, D., Benhamou, M., Andremont, A., Velasco, I.T., Chiamolera, M., Verbeek, J.S., Launay, P., and Monteiro, R.C. (2007). CD16 promotes Escherichia coli sepsis through an FcR gamma inhibitory pathway that prevents phagocytosis and facilitates inflammation. Nat. Med. *13*, 1368–1374.

Pinheiro da Silva, F., Aloulou, M., Benhamou, M., and Monteiro, R.C. (2008). Inhibitory ITAMs: a matter of life and death. Trends Immunol. *29*, 366–373.

Pleass, R.J., Dunlop, J.I., Anderson, C.M., and Woof, J.M. (1999). Identification of residues in the CH2/CH3 domain interface of IgA essential for interaction with the human fcalpha receptor (FcalphaR) CD89. J. Biol. Chem. *274*, 23508–23514.

Reth, M. (1989). Antigen receptor tail clue. Nature *338*, 383–384.

Rittirsch, D., Huber-Lang, M.S., Flierl, M.A., and Ward, P.A. (2009). Immunodesign of experimental sepsis by cecal ligation and puncture. Nat. Protoc. *4*, 31–36.

Rossato, E., Ben Mkaddem, S., Kanamaru, Y., Hurtado-Nedelec, M., Hayem, G., Descatoire, V., Vonarburg, C., Miescher, S., Zuercher, A.W., and Monteiro, R.C. (2015). Reversal of Arthritis by Human Monomeric IgA Through the Receptor-Mediated SH2 Domain-Containing Phosphatase 1 Inhibitory Pathway. Arthritis Rheumatol. *67*, 1766–1777.

Shen, L., Collins, J.E., Schoenborn, M.A., and Maliszewski, C.R. (1994). Lipopolysaccharide and cytokine augmentation of human monocyte IgA receptor expression and function. J. Immunol. *152*, 4080–4086.

Singer, M., Deutschman, C.S., Seymour, C.W., Shankar-Hari, M., Annane, D., Bauer, M., Bellomo, R., Bernard, G.R., Chiche, J.D., Coopersmith, C.M., et al. (2016). The Third International Consensus Definitions for Sepsis and Septic Shock (Sepsis-3). JAMA *315*, 801–810.

Takeda, K., and Akira, S. (2001). Roles of Toll-like receptors in innate immune responses. Genes Cells *6*, 733–742.

Teupser, D., Weber, O., Rao, T.N., Sass, K., Thiery, J., and Fehling, H.J. (2011). No reduction of atherosclerosis in C-reactive protein (CRP)-deficient mice. J. Biol. Chem. *286*, 6272–6279.

Van Avondt, K., van Sorge, N.M., and Meyaard, L. (2015). Bacterial immune evasion through manipulation of host inhibitory immune signaling. PLoS Pathog. *11*, e1004644.

van Egmond, M., van Garderen, E., van Spriel, A.B., Damen, C.A., van Amersfoort, E.S., van Zandbergen, G., van Hattum, J., Kuiper, J., and van de Winkel, J.G. (2000). FcalphaRI-positive liver Kupffer cells: reappraisal of the function of immunoglobulin A in immunity. Nat. Med. *6*, 680–685.

Watanabe, T., Kanamaru, Y., Liu, C., Suzuki, Y., Tada, N., Okumura, K., Horikoshi, S., and Tomino, Y. (2011). Negative regulation of inflammatory responses by immunoglobulin A receptor (FcαRI) inhibits the development of Toll-like receptor-9 signalling-accelerated glomerulonephritis. Clin. Exp. Immunol. *166*, 235–250.

STAR★METHODS

KEY RESOURCES TABLE

REAGENT or RESOURCE	SOURCE	IDENTIFIER
Antibodies		
Rabbit anti-SHP-1 (C-19)	Cliniscience	Cat# sc-287; RRID:AB_2173829
Rabbit anti-Syk (4D10)	Cliniscience	Cat# sc-1240; RRID:AB_628308
Anti-human TLR1 PE	eBioscience	Cat# 12-9911-42; RRID:AB_1272081
Anti-human TLR2 FITC	IMGENEX	Cat# IMG-416C; RRID:AB_317469
Anti-human TLR3 PE	Invitrogen	Cat# MA5-16188; RRID:AB_2537707
Anti-human TLR4 FITC	IMGENEX	Cat# IMG-417C; RRID:AB_317490
Anti-human TLR5 PE	IMGENEX	Cat# IMG-663D; RRID:AB_614264
Anti-human TLR6 PE	IMGENEX	Cat# IMG-304D; RRID:AB_1152366
Anti-human TLR7 FITC	IMGENEX	Cat# IMG-665C; RRID:AB_1152384
Anti-human TLR8 PE	IMGENEX	Cat# IMG-321D; RRID:AB_317509
Anti-mouse CD16/CD32 APC/Cy7	BioLegend	Cat# 101327; RRID:AB_1967102
Anti-mouse CD64 APC	BioLegend	Cat# 139305; RRID:AB_11219205
Anti- mouse CD16.2 PE (clone: 9E9)	BioLegend	Cat# 149504; RRID:AB_2565811
Mouse anti-CD89 PE (clone: A59)	BD PharMingen	Cat# 555686; RRID:AB_396037
Anti-human Mannose APC	BioLegend	Cat# 321110; RRID:AB_571885
Rabbit anti-Marco	Santa-cruz	Cat# sc-68913; RRID:AB_2140586
Goat anti-human IgA FITC	Southern Biotech	Cat# 2050-02; RRID:AB_2795702
Rat anti-mouse IgA FITC	BD PharMingen	Cat# 559354; RRID:AB_397235
Mouse anti-CD89 (MIP-8a)	BIO-RAD	Cat# MCA1824; RRID:AB_322934
Mouse anti-CD89 (clone A3)	Home made	N/A
Mouse anti-CD89 (clone A77)	Home made	N/A
Anti-mouse-CD11-c APC-Cy7	BD PharMingen	Cat# 561241; RRID:AB_10611727
Mouse IgG1 isotype PE	BD PharMingen	Cat# 555749; RRID:AB_396091
Armenian Hamster IgG PE	BioLegend	Cat# 400907; RRID:AB_326593
Mouse IgG1 Alexa-647	BioLegend	Cat# 400130; RRID:AB_400130
Mouse IgG APC	BioLegend	Cat# 400120
Armenian Hamster IgG1, λ2	BD PharMingen	Cat# 117309
Ns-IgA	MP biomedical	Cat# 55906
Pd-IgA	CSL Behring	N/A
Goat anti–rabbit IgG HRP	GE Healthcare	Cat# 65-6120; RRID:AB_88384
Bacterial and Virus Strains		
E. coli K12	ATCC	Cat# MG1655; RRID:Addgene_61440
S. pneumoniae	ATCC	Ca# 6303
S. aureus	ATCC	Cat# 25923
S. pyogenes	Pasteur institut	Cat# CIP 56.41T
E. coli WzxE$^{-/-}$	Yale university	N/A
E. coli K12 Texas-red	ThermoFisher Scientific	Cat# E2863
E. coli K12 pHrodo	ThermoFisher Scientific	Cat# P35361
Biological Samples		
Blood from CVID patients	Saint-Louis hospital	N/A
Chemicals, Peptides, and Recombinant Proteins		
Soluble CD89 (sCD89)	Sigma aldrich	KK5121

(*Continued on next page*)

Continued

REAGENT or RESOURCE	SOURCE	IDENTIFIER
Critical Commercial Assays		
Mouse IL-1 Elisa Kit	R&D system	Cat# DY401-05
Mouse IL-6 Elisa Kit	R&D system	Ca# DY406-05
Mouse TNF alpha Elisa Kit	R&D system	Cat# DY410
Human IL-1 Elisa Kit	R&D system	Cat# DY201
Human IL-6 Elisa Kit	R&D system	Cat# DY206
Human TNF alpha Elisa Kit	R&D system	Cat# DY210
Dynabeads Untouched Human Monocytes Kit	ThermoFisher Scientific	Cat# 11350D
Oligonucleotides		
Il-1 (NM_008361) Forward	Eurofins	5′CAACCAACAAGTGATATTCTCCATG-3′
Il-1 (NM_008361) Reverse	Eurofins	5′GATCCACACTCTCCAGCTGCA-3′
Il-1 (NM_008361) Probe	Eurofins	5′CTGTGTAATGAAAGACGGCACACCCACC −3′
Il-6 (NM_031168) Forward	Eurofins	5′TCCTACCCCAATTTCCAATGC-3′
Il-6 (NM_031168) Reverse	Eurofins	5′TGAATTGGATGGTCTTGGTCCT −3′
Il-6 (NM_031168) Probe	Eurofins	5′CAGATAAGCTGGAGTCACAGAAGGAGTGG −3′
TNF-alpha (NM_013693) Forward	Eurofins	5′CATCTTCTCAAAATTCGAGTGACAA −3′
TNF-alpha (NM_013693) Reverse	Eurofins	5′TGGGAGTAGACAAGGTACAACCC −3′
TNF-alpha (NM_013693) Probe	Eurofins	5′CACGTCGTAGCAAACCACCAAGTGGA −3′
Primer: ec1tgCD89	This paper	5′GGGGAATTCGACGCAAACAAGGCAGGGCGC −3
Primer: Cy21tgCD89	This paper	5′GGGGTCGACCTTGCAGACACTTGGTGTTCG −3
Software and Algorithms		
Fiji/ImageJ	National Institutes of Health	https://imagej.nih.gov/ij/docs/guide/146-2.html; RRID:SCR_002285; RRID:SCR_003070
GraphPad Prism	GraphPad Software	RRID:SCR_002798
FACSDiva	Becton Dickinson	N/A
FlowJo	Becton Dickinson	RRID:SCR_008520
IDEAS v6	AMNIS	N/A
Other		
Todd Hewitt Broth media	Becton Dickinson	Cat# 221714
Luria-Bertani	ThermoFisher Scientific	Cat# 11758902
Columbia CNA agar	Becton Dickinson	Cat# PA257303.04
Drigalski agar	Becton Dickinson	Cat# PA256500.06
5,6-carboxyfluorescein succinimidyl ester	ThermoFisher Scientific	Cat# 46409
Yeast extract	Becton Dickinson	Cat# 212750
Mouse GM-CSF	Peprotech	Cat# 300-03
Mouse IL-4	Peprotech	Cat# 200-04
Colony-stimulating factor1	R&D system	Cat# Q3U4F9

CONTACT FOR REAGENT AND RESOURCE SHARING

Further information and request for resources and reagents should be directed to and will be fulfilled by the Lead Contact, Sanae Ben Mkaddem (sanae.benmkaddem@inserm.fr).

EXPERIMENTAL MODEL AND SUBJECT DETAILS

Subjects

Eight patients with common variable immunodeficiency disorders (CVID) based on the criteria used for the diagnosis of CVID consistent with the European Society for Immunodeficiencies/Pan-American Group for Immunodeficiency criteria (Conley et al., 1999) were included in this study. Patients studied were selected with IgG replacement for the present study. Serum IgA levels were < 0.05 g/l (Table S1). The study was approved by the French ethic committees'' Comité Consultatif pour la protection des personnes dans

la recherché biomedicale, Ile de France-Paris-St ANTOINE),'' the approval number is 04579 and all human participants provided written informed consent. Blood from seven healthy donors was obtained from the Etablissement Français du Sang (Saint Louis hospital).

Animals

Female C57BL/6 $CD89^{Tg}$ mice expressing the wild-type human CD89 on monocytes and/or macrophages under the control of the CD11b promoter as well as mice expressing the R209L mutant of CD89 under control of the same promoter ($CD89_{R209L}{}^{Tg}$) all aged 8-12 weeks were used, as previously described (Kanamaru et al., 2007; Launay et al., 2000). As mice do not express homologs of CD89, non-transgenic littermates served as negative controls. Of note, mouse IgA does not bind effectively CD89 (Pleass et al., 1999; Berthelot et al., 2012). CD16-KO mice were from the Jackson Laboratory and the $CD89^{Tg}$CD16-KO were obtained by backcrossing of CD16-KO and $CD89^{Tg}$. C-reactive protein (CRP) knock-out mice have been previously described (Teupser et al., 2011). All strains were maintained at the animal facility of Bichat Medical School. All experiments were performed in accordance with the French Council of Animal Care guidelines and national ethical guidelines of Paris-Nord Animal Care Committee (Animal Use Protocol number APAFIS#14243-2018032217215463 v8).

METHOD DETAILS

Pneumonia and cecal ligation and puncture models

Pneumonia was induced by intranasal administration of 5.10^5 CFU of *S. pneumoniae Pn3* (ATCC-6303, Manassas, USA) in mice under isoflurane anesthesia (Baxter, France). Paraffin-embedded lung sections were obtained and stained with H&E for morphological analysis. Peritonitis was induced by CLP as described (Pinheiro da Silva et al., 2007; Rittirsch et al., 2009). Briefly, mice were anesthetized using ketamine and xylasine (Virbac, France). After anesthesia, the abdomen was shaved, and the cecum exposed through a 1-cm midline incision. The cecum was ligated between the 3rd and 4th vascular arcade with a 4-0 silk suture (Ethicon, France) and punctured twice with a 21-gauge needle. Recovery was facilitated by placing mice on a heated pad. Blood was collected by cardiac puncture, and hematological parameters were monitored using a MS9 analyzer (Melet Schloesing, France). Time to death was recorded during the following 7 days, when surviving mice were euthanized.

Cells, reagents and antibodies

In mouse experiments, bone-derived mouse macrophages (BMM) were obtained after a 7-day culture of bone marrow cells from 8 to 12-week-old mice in the presence of colony-stimulating factor1 (R&D system, France). In *ex-vivo* human blood cell experiments, peripheral blood mononuclear cells (PBMC) were first isolated by using Ficoll gradients followed by a negative selection for monocytes using Dynabeads Untouched Human Monocytes Kit (Invitrogen, France). Monocytes were cultured in RPMI supplemented with glutamate (Invitrogen, France) and 10% fetal bovine serum (Invitrogen, France) for 5 days to generate macrophages.

BMDCs were generated from 6-8 week-old wild-type and $CD89^{Tg}$ mice. Briefly, a cell suspension was prepared from BM obtained from femurs and tibias. After lysing red blood cells, whole BM cells (2 × 106 cells/mL) were cultured in RPMI 1640 medium in six-well flat bottom plates (Orange Scientific, Braine-l'Alleud, Belgium) at 37°C, 5% CO2, supplemented with 10% fetal calf serum (FCS), 2 mM L-glutamine, 100 U/mL penicillin G, 100 mg/mL streptomycin, 30 ng/mL reconstructive mouse GM-CSF (Peprotech, Rocky Hill, USA) and 20 ng/mL reconstructive mouse IL-4 (Peprotech, Rocky Hill, USA). Cells were incubated for 24 h. Plates were then gently swirled and the medium containing non-adherent cells was removed and replaced with nutrient medium as described above. Supplemented medium was replaced every three days. Cell differentiation was assessed by flow-cytometry staining using anti-CD11c (N418) and anti-CD11b (M1/70) (BD Biosciences; each at 2 μg/ml).

Anti-CD89 (clone A59)-phycoerythrin (PE) conjugate was purchased from Becton Dickinson. Unconjugated MIP8a anti-CD89 was purchased from (ABD Serotec) and digested by pepsin to generate $F(ab')_2$ fragments as described (Aloulou et al., 2012). Human monomeric plasma derived IgA (pd-IgA) from one thousand healthy donors was kindly provided by CSL behring. Of note, the pd-IgA preparation was purified from the same batch that contain IVIg antibodies reacting to different bacteria which was efficient against infection in CIVD patients (Lucas et al., 2010). Non-specific human monomeric IgA (ns-IgA) was purchased from (MP biomedicals, France).

The *Escherichia coli* (*E. coli*-K12, Strain SMG 123 (PTA-7555)), *Staphylococcus aureus* subsp. aureus Rosenbach (*S. aureus*, ATCC® 25923), *Streptococcus pyogenes* Rosenbach (*S. pyogenes*, ATCC® 19615) and *Escherichia coli*-K12 WzxE (Coli genetic stock center, Yale university) were used for sCD89-bacteria interaction assays shown in Figure 1C.

Flow cytometry

Expression of CD89 was quantified on cells using flow cytometry. Cells were preincubated or not with 100 μg human IgG to block FcγRs for 15 min before incubation with labeled mAbs or irrelevant mAb for 30 min at 4°C. After washing, cells were analyzed by FACSfortessa flow cytometer (Becton Dickinson). Results were analyzed using the FlowJo software (Ashland, OR, USA). Receptor expression was represented by the ratio of mean fluorescence intensity (MFI) of receptor/ MFI of isotype control.

Imaging flow cytometry

BMDCs were generated as described above. BMDCs were washed and incubated, in the absence of fetal bovine serum, with Texas-red labeled *E. coli* () for 2h at 37°C. Cells were fixed with PFA 2% then anti-mouse CD11c (BD Biosciences) were used for membrane staining. BMDCs were gated as Singlets cells/Focus high/CD11c high. *E. coli* staining (Texas-Red) was determined for each BMDCs as the ratio of the geometric mean of their *E. coli* intensity on the mean BMDCs CD11c FMO (Fluorescence Minus One) intensity. Phagocytosis scores were determined using CD11c staining as a membrane marker and *E. coli* staining as the probe. All analyses were performed using the ImageStream X Mark II imaging flow cytometer and the IDEAS v6 software (AMNIS) (Figure 4).

Protein expression on BMM membrane

Protein expression of TLRs and of MARCO was quantified on BMM using flow cytometry. Anti TLR antibodies were obtained from Imgenex (Clinisciences, Nanterre, France), including anti-TLR1 phycoerythrin (PE) conjugate, anti-TLR2 Fluorescein isothiocyanate (FITC) conjugate anti-TLR3 phycoerythrin (PE) conjugate, anti-TLR4 Fluorescein isothiocyanate (FITC) conjugate, anti-TLR5 phycoerythrin (PE) conjugate, anti-TLR6 phycoerythrin (PE) conjugate, anti-TLR8 phycoerythrin (PE) conjugate. Anti-MARCO antibodies were obtained from Santa Cruz (Heidelberg, Germany). Isotype controls were obtained from Becton Dickinson. BMM were stained with anti-extracellular antibodies for 30 minutes at 4°C. A total of 10000 viable PBMC were collected using BD FACSDiva Software by flow cytometry (FACSCanto II, Becton Dickinson, France). Results were analyzed using the FlowJo software (Ashland, OR, USA). TLR expression is represented by the ratio of mean fluorescence intensity (MFI) of TLR / MFI of isotype control.

Bacteria and microbiological culture

Serotype 3 *S. pneumoniae*, was grown in Todd Hewitt Broth media (Becton Dickinson, France) supplemented by 0.5% yeast extract (Becton Dickinson, France) at 37°C, to midlog phase. Strain K-12 MG1655 is a laboratory-derived commensal *E. coli* strain. It belongs to the A phylogenetic group and has no resistance to antibiotics or virulence factors. The K-12 *E. coli* strain was grown in Luria–Bertani (Becton Dickinson, France) broth at 37°C, to midlog phase. *Streptococcus pyogenes* (CIP 56.41T, Pasteur Institute, France) was grown in Todd Hewitt Broth media supplemented by 0.5% yeast extract at 37°C, to midlog phase. Bacteria were pelleted by centrifugation (16,000 x g for 10 minutes), washed twice in endotoxin-free PBS (Invitrogen). Bacteria concentration was determined spectrophotometrically (A600) and then confirmed by plating serially diluted bacteria on respectively soy-based blood agar plates (Becton Dickinson, France) and Luria–Bertani agar plates.

Bacterial invasion count

Pneumonia model: lungs were harvested and then homogenized with a tissue blender (Ultra-Turrax T25, Fisher Scientific, France) in one milliliter of 0.9% sodium chloride during 1 minute. Bacterial counts were determined by plating serial dilutions of the homogenate on soy-based blood agar plates (Becton Dickinson, France).

Cecal ligation and puncture model: peritoneal fluid was serially diluted, and subsequently spread on Luria–Bertani agar plates (Becton Dickinson, France) and bacteria-selective agar plates. Plates were incubated in aerobic conditions for 1 day. *E. coli* selective medium was Drigalski agar (Becton Dickinson, France), *Enterococcus* were detected and quantified using Columbia CNA agar (Becton Dickinson, France) and identified by MALDI-TOF technique. Results are expressed as log CFU/organ.

Bacterial binding and phagocytosis assays

10^6 BMM were washed and incubated, in the absence of fetal bovine serum, with Texas-red labeled *E. coli* (Molecular Probes) or 10^7 CFU 5,6-carboxyfluorescein succinimidyl ester (FAM-SE; Molecular Probes, Thermo Fisher, France) labeled *S. pneumoniae* (Martinez et al., 1999) for 30 minutes at 4°C for the binding assays or 37°C for the phagocytosis assays, respectively. The staining of WGA (4 μg/ml in PBS) was performed on fixed cells with 4% of PFA and after bacteria binding or phagocytosis assays. Slides were mounted and examined by confocal laser scanning microscopy with a CLSM-510-META microscope (Carl Zeiss, France).

For *E. coli* phagocytosis assay in BMM derived from $CD89^{Tg}$ animals or littermates, we used the pHrodo dye labeling system, in which pHrodo label of internalized bacteria dramatically increase in fluorescence at the acidic pH found in phago-lysosomes giving a good quantitative index of bacteria phagocytosis.

Bacterial killing

To measure intracellular bacterial killing, in the absence of fetal bovine serum, we incubated live *E. coli* (ATCC no. 25922) with cells (10^7 bacteria per $5x10^5$ cells) at 37°C for 30 min. We removed unbound bacteria by differential centrifugation (Leijh et al., 1979) and suspended the pellets in gentamicin solution (100 μg/ml from Sigma-Aldrich, St. Louis, MO), which we incubated for 2h at 37°C to kill any extracellular bacteria. After rinsing in PBS, cells were either lysed by incubation on ice with 0.5% Triton X-100 for 10 min or incubated at 37°C for 30 and 60 min before lysis under the same conditions (Leijh et al., 1979). We counted the surviving bacteria on selective agar plates.

Confocal laser scanning microscopy

The production of reactive oxygen species by BMM was measured by imaging microscopy. BMM were plated on Lab-Tek chambered coverglass slides (Thermo Fisher scientific, France) and loaded with 50 μM DCFH-DA (Invitrogen, France) for 30 minutes. Cells

were then rinsed and stimulated with 10^{-8} of fMLF. After excitation at 488 nm, the green fluorescence of DCF was measured by confocal laser scanning microscopy with CLSM-510-META microscope (Carl Zeiss, France) equipped with a cell culture chamber at 37°C, under 5% CO_2 atmosphere.

ROS production assay on PMN by chemiluminescence

After isolation, PMNs were suspended in Hank's Balanced Salt Solution (Life technologies, France) to reach a concentration of 10^6 cells per ml and left to rest for 30 minutes at room temperature. fMLF (Sigma-Aldrich, France) and Luminol (Sigma-Aldrich, France) were diluted 1:100 in Hank's Balanced Salt Solution and kept on ice. Luminol (Sigma-Aldrich, France) was protected from light by aluminum foil. Five hundred μl of the solution containing PMNs were added to each of 6 tubes followed by the addition of Luminol and 10 minutes incubation at 37°C in the chamber of a luminometer (Berthold–Biolumat LB937, France). Changes in chemiluminescence were then measured over 30 minutes after stimulation with *E. coli*, *S. pneumoniae* or with fMLF.

Immunoprecipitation and immunoblotting

Cells were solubilized in lysis buffer containing 1% Nonidet P-40, 0.1% sodium dodecyl sulfate (SDS) (Sigma-Aldrich, France). For immunoprecipitation, cell lysates were incubated with A77 anti-CD89 mAb and immunoprecipitated overnight at 4°C with Protein G-Sepharose beads (GE Healthcare, France) as described (Ben Mkaddem et al., 2014). Samples were resolved by SDS–10% polyacrylamide gel electrophoresis, transferred onto nitrocellulose membranes and immunoblotted with rabbit anti-Syk (Santa Cruz Biotechnology, USA) or rabbit anti–SHP-1 (Santa Cruz Biotechnology, USA) antibodies followed by goat anti–rabbit IgG (GE Healthcare, France) coupled to horseradish peroxidase. Membranes were developed by enhanced chemical luminescence treatment (Amersham Biosciences, France).

Production of soluble proteins and antibodies

Soluble CD89 was expressed and produced in lytic baculovirus/insect cell expression systems (home-made as described; Berthelot et al., 2012). Mouse IgG1 anti-CD89 mAbs (clones A3 and A77) were produced and purified in our laboratory as described (Monteiro et al., 1992). A3 and A77 were used for ELISA.

ELISA

Regarding cytokine and chemokine assays, mouse TNF-α, IL-1 and IL-6 levels were measured by ELISA, following the manufacturer's instructions (R&D Systems, France). Regarding binding assays, plates were coated overnight with 10^5, 10^6, 10^7, 10^8 chemically killed bacteria in 100 μL of sterile PBS. Wells were then blocked with milk 2% for 2h. Recombinant soluble CD89 in PBS was incubated for 2h. After washing, the biotinylated A3 mAb anti-CD89 was added followed by streptavidin alkaline phosphatase (Becton Dickinson, France). The reaction was developed by adding the alkaline phosphatase substrate (Sigma-Aldrich, France) for 1 hour and measured at 405nm. As a negative control, plates coated with only albumin were used. Competitive ELISA assays between human IgA, bacteria and soluble recombinant CD89 were undertaken using human IgA (MP Biomedicals, France) and human IgG (TEGELINE, LFB Biomedical, les ULIS France) as a control. Briefly, 50μg/ml of sCD89 was incubated with different concentrations of serum IgA for 30 minutes. Then the complex was added on plates coated with 10^6 bacteria and incubated for another 2h at 37°C. After washing, the biotinylated A3 mAb anti-CD89 was added followed by streptavidin alkaline phosphatase (Becton Dickinson, France) and the reaction was developed as described above.

Real-time PCR

RNA purification from homogenized kidneys was performed by using RNAble (Eurobio). cDNA was obtained by reverse transcription using Moloney murine leukemia virus reverse transcriptase (Invitrogen, France). Samples were analyzed by real-time PCR with TaqMan® Gene Expression Master Mix (Invitrogen, France). Gene quantification was performed using a Chromo4 Real-Time PCR Detection System (Bio-Rad Laboratories, France). Data were normalized to β-actin mRNA values.

QUANTIFICATION AND STATISTICAL ANALYSIS

All data were obtained using cells from at least three independent culture preparations or at least three independent animals per genotype. Repeats for experiments and statistical tests carried out are given in the figure legends as N numbers and refer to number of cells unless otherwise stated. Statistical analysis was performed using the Graphpad Prism v7.00 software (GraphPad Software, Inc., La Jolla, CA, USA). Mann-Whitney tests were performed for between-group comparisons. Survival differences were determined using the Kaplan-Meier method and the Log-rank test. All tests were two-tailed. (not significant [ns], $p > 0.05$; * $p < 0.05$; ** $p < 0.01$; *** $p < 0.001$).